

Numerical renormalization group calculation of impurity internal energy and specific heat of quantum impurity models

L. Merker¹ and T. A. Costi¹

¹*Peter Grünberg Institut and Institute for Advanced Simulation, Research Centre Jülich, 52425 Jülich, Germany*
(Dated: March 8, 2013)

We introduce a method to obtain the specific heat of quantum impurity models via a direct calculation of the impurity internal energy requiring only the evaluation of local quantities within a single numerical renormalization group (NRG) calculation for the total system. For the Anderson impurity model, we show that the impurity internal energy can be expressed as a sum of purely local static correlation functions and a term that involves also the impurity Green function. The temperature dependence of the latter can be neglected in many cases, thereby allowing the impurity specific heat, C_{imp} , to be calculated accurately from local static correlation functions; specifically via $C_{\text{imp}} = \frac{\partial E_{\text{ionic}}}{\partial T} + \frac{1}{2} \frac{\partial E_{\text{hyb}}}{\partial T}$, where E_{ionic} and E_{hyb} are the energies of the (embedded) impurity and the hybridization energy, respectively. The term involving the Green function can also be evaluated in cases where its temperature dependence is non-negligible, adding an extra term to C_{imp} . For the non-degenerate Anderson impurity model, we show by comparison with exact Bethe ansatz calculations that the results recover accurately both the Kondo induced peak in the specific heat at low temperatures as well as the high temperature peak due to the resonant level. The approach applies to multiorbital and multichannel Anderson impurity models with arbitrary local Coulomb interactions. An application to the Ohmic two state system and the anisotropic Kondo model is also given, with comparisons to Bethe ansatz calculations. The approach could also be of interest within other impurity solvers, for example, within quantum Monte Carlo techniques.

PACS numbers: 75.20.Hr, 71.27.+a, 72.15.Qm

I. INTRODUCTION

Quantum impurity models play an important role in condensed matter physics, for example, as models of transition metal and rare-earth impurities in metals¹ or two-level systems^{2–6} and qubits⁷ interacting with an environment or in describing the Kondo effect in nanoscale devices such as molecular transistors,^{8–11} semiconductor quantum dots,^{12–14} carbon nanotubes,¹⁵ and magnetic ions such as Co^{16,17} or Ce¹⁸ adsorbed on surfaces. In addition, they appear as the effective models within dynamical mean field theory (DMFT) treatments of strongly correlated electron systems, such as heavy fermions and transition metal oxides.^{19–22} Hence, new approaches to calculate their dynamic, thermodynamic and transport properties are potentially of wide interest.

The numerical renormalization group (NRG) method,^{23–26} in particular, has proven very successful for the study of quantum impurity models. The method, described briefly in the next section, gives both the thermodynamic,^{23–25,27} dynamic,^{28–35} and transport properties³⁶ of quantum impurities. Thermodynamic properties, such as the specific heat, are of particular interest for bulk systems, such as dilute concentrations of transition metal or rare-earth ions in non-magnetic metals.¹ A measurement of the temperature dependence of the specific heat or susceptibility of such systems provides important information about their physical behavior, for example, whether such systems exhibit Fermi liquid or non-Fermi liquid behavior at low temperature and thus information about the nature of their low energy excitations.^{37,38}

The usual approach to calculating the specific heat of quantum impurity models within the NRG method consists of a two-stage procedure,^{24–27} in which the Hamiltonians of the total system H is first diagonalized, followed by a similar diagonalization for the host Hamiltonian H_0 . Here, $H = H_{\text{imp}} + H_{\text{int}} + H_0$ is the Hamiltonian of a quantum impurity (described by H_{imp}), interacting with a host (described by H_0) via the interaction term H_{int} . From the eigenvalues of H and H_0 , the grand canonical partition functions $Z = \text{Tr } e^{-\beta H}$ and $Z_0 = \text{Tr } e^{-\beta H_0}$ and the corresponding thermodynamic potentials $\Omega(T) = -k_B T \ln Z$ and $\Omega_0(T) = -k_B T \ln Z_0$ are constructed, where $\beta = 1/k_B T$ is the inverse temperature. The impurity contribution to the specific heat, $C_{\text{imp}}(T)$, is then obtained by subtraction via $C_{\text{imp}}(T) = C(T) - C_0(T)$, where $C(T)$ and $C_0(T)$ are the specific heats of the total system and of the host system, respectively,

$$C(T) = -T \frac{\partial^2 \Omega(T)}{\partial T^2} = k_B \beta^2 \langle (H - \langle H \rangle)^2 \rangle, \quad (1)$$

$$C_0(T) = -T \frac{\partial^2 \Omega_0(T)}{\partial T^2} = k_B \beta^2 \langle (H_0 - \langle H_0 \rangle)^2 \rangle \quad (2)$$

$$C_{\text{imp}}(T) = C(T) - C_0(T). \quad (3)$$

In this paper we present a new approach to the calculation of the impurity internal energy and specific heat of quantum impurity models within the numerical renormalization group (NRG) method.^{23–26} It relies on expressing the impurity internal energy in terms of local quantities, and as such is not restricted to the NRG but may be implemented within any impurity solver that calculates such quantities. The main result of this paper is

the (approximate) expression for the impurity specific heat of the Anderson model (see Sec. III)

$$C_{\text{imp}}(T) = \frac{\partial E_{\text{ionic}}}{\partial T} + \frac{1}{2} \frac{\partial E_{\text{hyb}}}{\partial T}, \quad (4)$$

where $E_{\text{ionic}} = \langle H_{\text{imp}} \rangle$ and $E_{\text{hyb}} = \langle H_{\text{int}} \rangle$. The main advantages of this approach are that, (i), Eq. (4) involves only a first temperature derivative and is expected to be more accurate for numerical evaluations than Eqs. (1)-(3) which involve a second temperature derivative of the thermodynamic potential, or, the calculation of the total energy fluctuation, (ii), the host contribution to the internal energy $\langle H_0 \rangle$ has been analytically subtracted out (see Sec. III), so only the diagonalization of H is required, (iii), only local static correlation functions appearing in $\langle H_{\text{imp}} \rangle$ and $\langle H_{\text{int}} \rangle$ are required, and, (iv), as we shall show, the new approach is less sensitive to discretization effects of the host than the usual approach which evaluates expectation values of extensive quantities. We illustrate the method by applying it to the Anderson impurity model and we compare the results for specific heats with those from the conventional NRG approach^{27,36,39} and with exact results from thermodynamic Bethe ansatz calculations.⁴⁰⁻⁴²

Early approaches to the specific heat of dilute Kondo systems used an equation of motion decoupling scheme for the Kondo model⁴³ and expressed the impurity internal energy in terms of the local T-matrix. The results obtained for the specific heat within this approximation were inadequate, violating, for example, Fermi liquid properties at low temperatures.⁴⁴ A formally exact expression for the internal energy of the Anderson model, in terms of the local self-energy and the local Green function, was obtained by Kj  llerstr  m et. al., in Ref. 45. They evaluated the specific heat in the low density limit (corresponding to a small occupation of the local level) obtaining correct results obeying Fermi liquid theory in this limit.

The most reliable approaches to specific heats of quantum impurity models are the Bethe ansatz method for integrable models^{40-42,46-49} and the NRG method. An important aspect of the latter, allowing it to access thermodynamic properties on all temperature scales down to $T = 0$, is the use of a logarithmic grid to represent the quasi-continuous spectrum $\omega \in [-D, +D]$ of the host system, H_0 . Thus $\omega \rightarrow \omega_n = \pm D\Lambda^{-n}$, $n = 0, 1, \dots$, where the parameter $\Lambda > 1$ achieves a separation of the many energy scales in H_0 and thus in H (see Sec. II). A large $\Lambda \gg 1$ allows calculations to reach low temperatures in fewer steps within the iterative diagonalization procedure of the NRG, and, in addition, a large $\Lambda \gg 1$ reduces the size of the truncation errors at each step in this procedure.²⁴ However, for $\Lambda \gg 1$, specific heats (and also susceptibilities), calculated by using a standard logarithmic grid, exhibit discretization oscillations, especially at low temperatures.⁵⁰ On the other hand, calculations at smaller $\Lambda \lesssim 3$, with less severe discretization oscillations, are more prone to truncation errors. In order

to be able to carry out accurate calculations at all temperatures, using $\Lambda \gg 1$, an averaging over several discretizations of the host degrees of freedom has been introduced which essentially allows exact calculations to be carried out.^{50,51} With this refinement, the NRG approach has been used extensively in calculations of specific heats of quantum impurity models,³⁹ with applications to the two-impurity Kondo model^{52,53} and the two-channel Anderson models.⁵⁴

The paper is organized as follows. In Sec. II, the Anderson impurity model is described, and the NRG is outlined together with a brief description of how thermodynamic properties are conventionally calculated within NRG (at $\Lambda \gg 1$). In Sec. III, we describe our new approach to specific heats of quantum impurity models, using the Anderson impurity model as an example (with some further details given in Appendix A). The availability of exact Bethe ansatz results for this model,⁴⁰⁻⁴² allows a detailed evaluation of the accuracy of our new approach to specific heats. Results at zero and finite magnetic fields are presented in Sec. IV for the symmetric Anderson model. These are compared to both exact Bethe ansatz results and results obtained in the conventional NRG approach. Sec. V contains results for the asymmetric model with comparisons to corresponding Bethe ansatz calculations. The thermodynamic Bethe ansatz (TBA) equations for the Anderson impurity model and the details of their numerical solution can be found in Appendix B. In Sec. VI we present the generalization to multichannel and multiorbital Anderson impurity models and to dissipative two state systems. For the Ohmic case, results for specific heats are compared to corresponding Bethe ansatz results for the equivalent anisotropic Kondo model (AKM). Section VII summarizes the main results of this paper and discusses possible future applications.

II. MODEL, METHOD AND CONVENTIONAL APPROACH TO THERMODYNAMICS

We consider the Anderson impurity model,⁵⁵ described by the Hamiltonian

$$H = H_{\text{imp}} + H_0 + H_{\text{int}}.$$

The first term, $H_{\text{imp}} = \sum_{\sigma} \varepsilon_d d_{\sigma}^{\dagger} d_{\sigma} + U n_{d\uparrow} n_{d\downarrow}$, describes the impurity with local level energy ε_d and on-site Coulomb repulsion U , the second term, $H_0 = \sum_{k\sigma} \varepsilon_k c_{k\sigma}^{\dagger} c_{k\sigma}$, is the kinetic energy of non-interacting conduction electrons with dispersion ε_k , and, the last term, $H_{\text{int}} = \sum_{k\sigma} V_k (c_{k\sigma}^{\dagger} d_{\sigma} + d_{\sigma}^{\dagger} c_{k\sigma})$, is the hybridization between the local level and the conduction electron states, with V_k being the hybridization matrix element. We shall also consider the effect of a magnetic field of strength B by adding a term $H_B = -g\mu_B B S_z$ to H where S_z is the z -component of the total spin (i.e., impurity plus conduction electron spin), g is the electron g -factor, and μ_B is the Bohr magneton. We choose units such that $g = \mu_B = 1$.

The NRG procedure consists of the following steps. First, the conduction electron energies $-D \leq \varepsilon_k \leq D$, where D is the half-bandwidth, are logarithmically discretized about the Fermi level $\varepsilon_F = 0$, that is, $\varepsilon_k \rightarrow \varepsilon_n = \pm D\Lambda^{-n}$, $n = 0, 1, \dots$ where $\Lambda > 1$ is a momentum rescaling factor. We shall also consider generalized discretizations defined by a parameter z , such that $\varepsilon_0 = \pm D$ and $\varepsilon_n = \pm D\Lambda^{-n-(1-z)}$, $n = 1, \dots$, with $z = 1$ recovering the usual discretization. For $\Lambda \gg 1$, discretization induced oscillations of period $\ln \Lambda$ can be eliminated by averaging results for several z in $(0, 1]$.^{50,51} Second, the operators $c_{n\sigma}$, $n = 0, 1, \dots$, are rotated to a new set $f_{n\sigma}$, $n = 0, 1, \dots$, with $Vf_{0\sigma} = \sum_{n=0}^{\infty} V_{kn} c_{n\sigma}$, such that the discretized conduction band $H_0 = \sum_{n=0}^{\infty} \pm E_n(z) c_{n\sigma}^\dagger c_{n\sigma}$, with, for example, $E_n(z) = \frac{1}{2}(1 + \Lambda^{-1})D\Lambda^{-n}$ for $z = 1$, takes the tri-diagonal form $H_0 \rightarrow \sum_{n=0}^{\infty} \tilde{\epsilon}_n(z) f_{n\sigma}^\dagger f_{n\sigma} + \sum_{n=0}^{\infty} t_n(z) (f_{n\sigma}^\dagger f_{n+1\sigma} + f_{n+1\sigma}^\dagger f_{n\sigma})$ in the new basis. Finally, within this new basis, the sequence of truncated Hamiltonians H_m , $m = 0, 1, \dots$, where $H_m = H_{\text{imp}} + H_{\text{hyb}} + \sum_{n=0}^m \tilde{\epsilon}_n(z) f_{n\sigma}^\dagger f_{n\sigma} + \sum_{n=0}^{m-1} t_n(z) (f_{n\sigma}^\dagger f_{n+1\sigma} + f_{n+1\sigma}^\dagger f_{n\sigma})$, with $H_{\text{hyb}} = V \sum_{\sigma} (f_{0\sigma}^\dagger d_{\sigma} + d_{\sigma}^\dagger f_{0\sigma})$, is iteratively diagonalized by using the recursion relation $H_{m+1} = H_m + \sum_{\sigma} \tilde{\epsilon}_{m+1}(z) f_{m+1\sigma}^\dagger f_{m+1\sigma} + \sum_{\sigma} t_m(z) (f_{m\sigma}^\dagger f_{m+1\sigma} + f_{m+1\sigma}^\dagger f_{m\sigma})$. This procedure²⁴⁻²⁶ yields the eigenstates $|p\rangle_m$ and eigenvalues E_p^m on a decreasing set of energy scales $\omega_m(z) \sim t_m(z)$, $m = 0, 1, \dots$. Since the number of states increases as 4^{m+2} , only the lowest states are retained for $m \geq m_0$, where typically $m_0 \geq 4 - 5$. This is implemented either by, (i), specifying an approximately constant number of states N_{keep} to retain at each $m \geq m_0$, and m_0 will be fixed by the precise value of N_{keep} , or, (ii), by specifying that only those states with rescaled energies $(E_p^m - E_{GS}^m)/t_m(z) < e_c(\Lambda)$ be retained for $m \geq m_0$, for some predefined m_0 , where E_{GS}^m is the (absolute) groundstate energy at iteration m and $e_c(\Lambda)$ is Λ -dependent cut-off energy. Combining the information from all iterations then allows the calculation of thermodynamics on all temperature scales of interest.^{39,50} For most of the results in this paper, we used the truncation scheme (ii) with $m_0 = 4 - 5$ and $e_c(\Lambda) = 20\sqrt{\Lambda}$, similar to the choice in Ref. 39. Some calculations using the truncation scheme (i) with $N_{\text{keep}} = 860$ were also carried out in Sec. VIB. Both schemes were found to work well by comparison with exact Bethe ansatz calculations. Whereas in scheme (i), a fixed number, N_{keep} , of levels is retained for all iterations $m \geq m_0$, in scheme (ii), the number of retained states, initially large for $m \lesssim m_0$ (typically several thousand), starts to decrease with increasing m , eventually saturating to a few hundred states at $m \gg m_0$ (e.g., for $\Lambda = 4$). While in both schemes only the retained states of iteration m are used to set up the Hamiltonian H_{m+1} for the next iteration, all states of iteration m are available, and are used, in practice, to calculate the thermodynamics.

The specific heat is calculated within the approach of Campo and Oliveira in Ref. 51, which we shall refer to as the “conventional” approach: For any temperature T ,

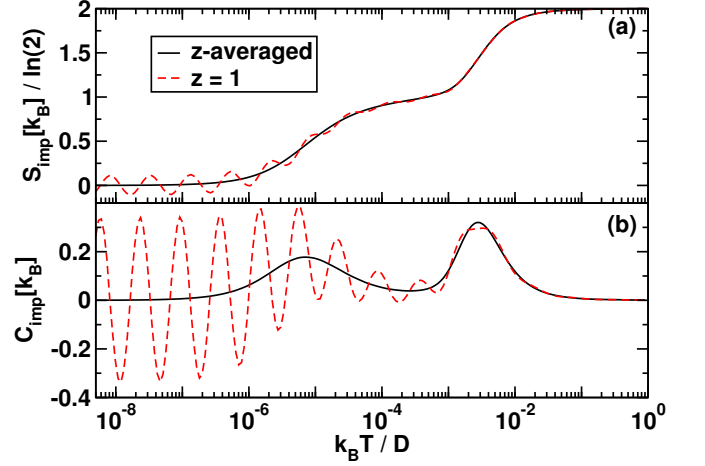


FIG. 1. (Color online) Temperature dependence of, (a), the impurity entropy, $S_{\text{imp}}(T)$, and, (b), the impurity specific heat, $C_{\text{imp}}(T)$, for the symmetric Anderson model with $U/\Delta_0 = 12$ and $\Delta_0 = 0.001D$. The calculations are for $\Lambda = 4$ with an energy cut-off $e_c(\Lambda = 4) = 40$, without z -averaging [$n_z = 1$, $z = 1$ (dashed lines)], and with z -averaging [$n_z = 2$, $z = 1/4, 3/4$ (solid lines)]. For $\Lambda = 4$ two z values suffice to eliminate the discretization oscillations.

we choose the smallest m such that $k_B T > t_m(z)$ and we use the eigenvalues of H_m to evaluate the partition function $Z_m(T) = \sum_p e^{-E_p^m/k_B T}$. The expectation value $\langle H \rangle$ is then calculated, followed by $\langle (H - \langle H \rangle)^2 \rangle$ and the specific heat $C(T)$ (in addition, the thermodynamic potential $\Omega(T) = -k_B T \ln Z_m(T)$ may also be calculated). Calculations are carried out for several values of the z parameter and then averaged. In the calculations reported below, we choose $z = (2i - 1)/2n_z$, $i = 1, \dots, n_z$ with $n_z = 2, 4$ or 8 . This procedure is repeated for the conduction band Hamiltonian H_0 to obtain the host contribution to the specific heat, $C_0(T)$. Finally, the impurity specific heat is obtained via $C_{\text{imp}}(T) = C(T) - C_0(T)$. The above prescription works well for $\Lambda \geq 4$, since the use of large Λ reduces the size of truncation errors during the iterative diagonalization of H and H_0 .²⁴ Furthermore, the use of large Λ , implies that the highest states of H_m have energies $\gg t_m(z) \sim T$ so that $Z_m(T)$ is a good approximation to the partition function of the infinite system at temperature T . In addition to the specific heat, we also calculate the impurity contribution to the entropy, $S_{\text{imp}}(T) = S(T) - S_0(T)$, where $S(T)$ and $S_0(T)$ are the entropies for H and H_0 , respectively, and

$$S(T) = -\frac{\partial \Omega}{\partial T} = k_B \ln Z(T) + \langle H \rangle / T, \quad (5)$$

$$S_0(T) = -\frac{\partial \Omega_0}{\partial T} = k_B \ln Z_0(T) + \langle H_0 \rangle / T. \quad (6)$$

Unless otherwise specified, the NRG calculations presented in this paper will be for a band of half-width $D = 1$ and a constant particle-hole symmetric density of states $N_F = 1/2D$. The hybridization strength, Δ_0 , defined as the half-width of the resonant level is given

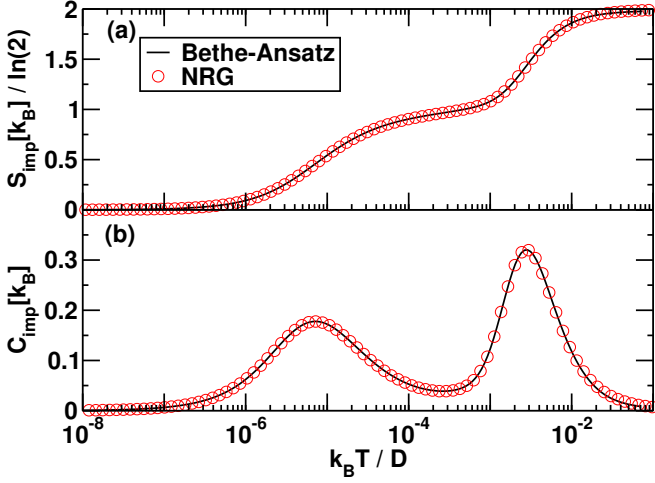


FIG. 2. (Color online) Temperature dependence of, (a), the impurity entropy, $S_{\text{imp}}(T)$, and, (b), the impurity specific heat, $C_{\text{imp}}(T)$, for the symmetric Anderson model with $U/\Delta_0 = 12$ and $\Delta_0 = 0.001D$. Symbols: NRG calculations using the conventional approach. Solid lines: Bethe ansatz calculations. The NRG calculations are z -averaged with $n_z = 2$ and other parameters as in Fig. 1.

by $\Delta_0 = \pi N_F V^2$. Calculations for the positive and negative- U Anderson models include a $U(1)$ symmetry for total electron number conservation and $SU(2)$ symmetry for total spin conservation. We use the discretization scheme of Campo and Oliveira in Ref. 51.

Figure 1 shows the temperature dependence of the specific heat and entropy, calculated with the above procedure, for the symmetric Anderson model with $U/\Delta_0 = 12$ and $\Delta_0 = 0.001D$. The calculations are for $\Lambda = 4$ using an energy cut-off $e_c(\Lambda = 4) = 40$, both without z -averaging ($n_z = 1$) and with z -averaging ($n_z = 2$). Note the aforementioned oscillations in the case of no z -averaging ($n_z = 1$). For $\Lambda = 4$, two z values suffice to eliminate the discretization oscillations (whereas for $\Lambda = 10$, four values are required). In order to quantify the accuracy of the NRG calculations, we also solved numerically the thermodynamic Bethe ansatz equations for the Anderson model and calculated the entropy and specific heat (see Appendix B for details). A comparison of the z -averaged NRG calculations with the exact Bethe ansatz results, shown in Fig. 2, indicates very good agreement. Nevertheless, in the next section we show that the specific heat can be calculated directly from the impurity contribution to the internal energy in terms of local static correlation functions and that discretization effects within this approach are less pronounced than those above.

III. IMPURITY INTERNAL ENERGY AND SPECIFIC HEATS

The impurity internal energy is defined by $E_{\text{imp}} = E_{\text{total}} - E_0$ where $E_{\text{total}} = \langle H \rangle$ and $E_0 = \langle H_0 \rangle = \sum_{k\sigma} \epsilon_k \langle c_{k\sigma}^\dagger c_{k\sigma} \rangle_0$, where the subscript 0 denotes a thermodynamic average for non-interacting conduction electrons (i.e., impurity is absent). We have

$$E_0 = \sum_{\sigma} \int d\epsilon f(\epsilon) \epsilon N(\epsilon), \quad (7)$$

where $f(\epsilon)$ is the Fermi function and $N(\epsilon) = \sum_k \delta(\epsilon - \epsilon_k)$ is the non-interacting conduction electron density of states per spin. E_{total} has four contributions:

$$E_{\text{total}} = E_{\text{occ}} + E_{\text{docc}} + E_{\text{cond}} + E_{\text{hyb}}, \quad (8)$$

where $E_{\text{occ}} = \sum_{\sigma} \epsilon_d \langle n_{d\sigma} \rangle$, $E_{\text{docc}} = U \langle n_{d\uparrow} n_{d\downarrow} \rangle$, $E_{\text{cond}} = \sum_{k\sigma} \epsilon_k \langle c_{k\sigma}^\dagger c_{k\sigma} \rangle$ and $E_{\text{hyb}} = V \sum_{k\sigma} \langle c_{k\sigma}^\dagger d_{\sigma} + d_{\sigma}^\dagger c_{k\sigma} \rangle$. The first two contributions are evaluated as thermodynamic averages within the NRG calculation, requiring the calculation of matrix elements of $\sum_{\sigma} n_{d\sigma}$ and the double occupancy operator $\hat{D}_{\text{occ}} = n_{d\uparrow} n_{d\downarrow}$. The contribution E_{hyb} may also be evaluated as a thermodynamic average $E_{\text{hyb}} = V \sum_{\sigma} \langle d_{\sigma}^\dagger f_{0\sigma} + H.c. \rangle$. For the discussion below it is useful to note that the contribution E_{hyb} can also be expressed in terms of the local retarded d-electron Green function $G_{d\sigma}(\omega) = \langle \langle d_{\sigma}; d_{\sigma}^\dagger \rangle \rangle_{\omega+i\delta}$ and the hybridization function $\Delta(\omega) = \sum_k V^2 / (\omega + i\delta - \epsilon_k)$ as

$$E_{\text{hyb}} = -\frac{2}{\pi} \sum_{\sigma} \int d\omega f(\omega) \text{Im} [G_{d\sigma}(\omega) \Delta(\omega)]. \quad (9)$$

Next, consider the contribution $E_{\text{cond}} = \sum_{k\sigma} \epsilon_k \langle c_{k\sigma}^\dagger c_{k\sigma} \rangle$. This is not simply E_0 since the impurity affects the conduction electrons once V is finite. It can be evaluated from the equation of motion of the retarded conduction electron Greens function $G_{k\sigma}(\omega) = \langle \langle c_{k\sigma}; c_{k\sigma}^\dagger \rangle \rangle_{\omega+i\delta}$:

$$G_{k\sigma} = G_{k\sigma}^0 + G_{k\sigma}^0 \mathcal{T}_{\sigma} G_{k\sigma}^0. \quad (10)$$

Here, $\mathcal{T}_{\sigma}(\omega) = V^2 G_{d\sigma}(\omega)$ is the local T-matrix and $G_{k\sigma}^0(\omega) = 1/(\omega + i\delta - \epsilon_k)$ is the non-interacting conduction electron Greens function. Using

$$\langle c_{k\sigma}^\dagger c_{k\sigma} \rangle = -\frac{1}{\pi} \int d\omega f(\omega) \text{Im} [\langle \langle c_{k\sigma}; c_{k\sigma}^\dagger \rangle \rangle]$$

we find for E_{cond}

$$E_{\text{cond}} = E_0 + E_{\text{int}},$$

where

$$\begin{aligned} E_{\text{int}} &= -\frac{1}{\pi} \sum_{\sigma} \int d\omega f(\omega) \int d\epsilon \text{Im} \left[\frac{\epsilon V^2 N(\epsilon)}{(\omega + i\delta - \epsilon)^2} G_{d\sigma}(\omega) \right] \\ &= -\frac{1}{\pi} \sum_{\sigma} \int d\omega f(\omega) \text{Im} [G_{d\sigma}(\omega) I(\omega)] \end{aligned}$$

where $I(\omega)$ is given by

$$I(\omega) = -\frac{1}{\pi} \int d\epsilon \frac{\epsilon \Delta_I(\epsilon)}{(\omega + i\delta - \epsilon)^2} = -\frac{\partial}{\partial \omega} (\omega \Delta(\omega))$$

with $\Delta_I(\epsilon) = \text{Im} [\Delta(\epsilon + i\delta)] = -\pi V^2 N(\epsilon)$, and we evaluated $I(\omega)$ analytically by noting that $\Delta(\omega + i\delta)$ has the same properties as a retarded Green function (see Appendix A for details). We therefore find,

$$E_{\text{int}} = \frac{1}{\pi} \sum_{\sigma} \int d\omega f(\omega) \text{Im} \left[G_{d\sigma}(\omega) \frac{\partial}{\partial \omega} (\omega \Delta(\omega)) \right] \\ = E_{\text{int}}^{(1)} + E_{\text{int}}^{(2)}, \quad (11)$$

$$E_{\text{int}}^{(1)} = \frac{1}{\pi} \sum_{\sigma} \int d\omega f(\omega) \text{Im} [G_{d\sigma}(\omega) \Delta(\omega)] \quad (12)$$

$$E_{\text{int}}^{(2)} = \frac{1}{\pi} \sum_{\sigma} \int d\omega f(\omega) \text{Im} \left[G_{d\sigma}(\omega) \omega \frac{\partial \Delta(\omega)}{\partial \omega} \right] \quad (13)$$

From this and Eq. (9) we see that $E_{\text{int}}^{(1)} = -\frac{1}{2} E_{\text{hyb}}$. Hence, the impurity contribution to the internal energy, $E_{\text{imp}} = E_{\text{total}} - E_0$, is given by

$$E_{\text{imp}} = E_{\text{occ}} + E_{\text{docc}} + \frac{1}{2} E_{\text{hyb}} + E_{\text{int}}^{(2)}, \quad (14)$$

$$= E_{\text{ionic}} + \frac{1}{2} E_{\text{hyb}} + E_{\text{int}}^{(2)}, \quad (15)$$

where $E_{\text{ionic}} = \langle H_{\text{imp}} \rangle = E_{\text{occ}} + E_{\text{docc}}$ is adiabatically connected to the energy of the impurity decoupled from the band (i.e., its energy at $V \rightarrow 0$). All contributions to E_{imp} , except for the last one, can be evaluated as thermodynamic averages of local static correlation functions: The contribution $E_{\text{int}}^{(1)}$ from the band which involves a finite frequency Greens function has been related to E_{hyb} , which can be evaluated as local static correlation function $V \sum_{\sigma} \langle d_{\sigma}^{\dagger} f_{0\sigma} + H.c. \rangle$. The contribution $E_{\text{int}}^{(2)}$, also involves a finite frequency Greens function, but we could not express this as a local static correlation function. Its temperature dependence, however, is negligible since the main temperature dependence arises from the Fermi window $|\omega| < T$, but this region is cut out in $E_{\text{int}}^{(2)}$ due to the factor of ω . In addition, for many cases of interest $\partial(\Delta(\omega))/\partial\omega$ is small and vanishes in the wide band limit: $D \rightarrow \infty$ and $\Delta_0 = \pi N(0)V^2$ fixed. For example, for a constant density of states it equals $\frac{2\Delta_0}{\pi D} (1 - (\omega/D)^2)^{-1} \sim \Delta_0/D$ for $\omega \ll D$. Thus, to a very good approximation, which we shall quantify in the rest of the paper with detailed numerical calculations and comparisons to exact Bethe ansatz results, we can approximate the impurity contribution to the specific heat and entropy via $\bar{E}_{\text{imp}} = E_{\text{ionic}} + \frac{1}{2} E_{\text{hyb}}$ as

$$C_{\text{imp}}(T) = \frac{\partial \bar{E}_{\text{imp}}}{\partial T} = \frac{\partial E_{\text{occ}}}{\partial T} + \frac{\partial E_{\text{docc}}}{\partial T} + \frac{1}{2} \frac{\partial E_{\text{hyb}}}{\partial T} \\ = \frac{\partial E_{\text{ionic}}}{\partial T} + \frac{1}{2} \frac{\partial E_{\text{hyb}}}{\partial T}, \quad (16)$$

$$S_{\text{imp}}(T) = \int_0^T dT' \frac{C_{\text{imp}}(T')}{T'}. \quad (17)$$

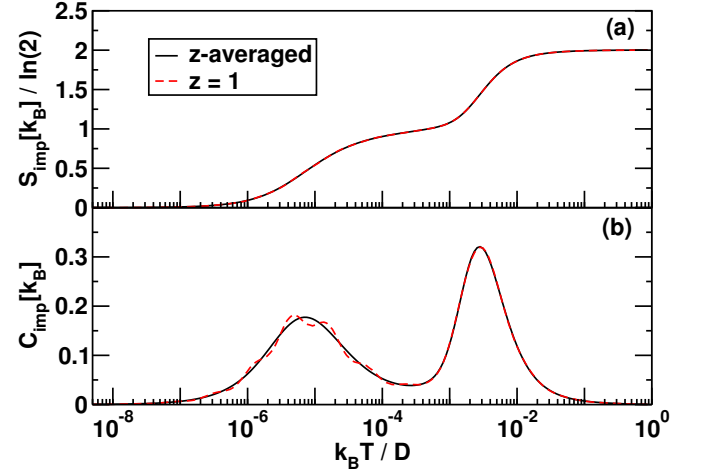


FIG. 3. (Color online) Temperature dependence of, (a), the impurity entropy, $S_{\text{imp}}(T)$, and, (b), the impurity specific heat, $C_{\text{imp}}(T)$, for the symmetric Anderson model with $U/\Delta_0 = 12$ and $\Delta_0 = 0.001D$ calculated within NRG using the new approach for $\Lambda = 4$ with an energy cut-off $e_c(\Lambda = 4) = 40$. Solid lines: $n_z = 2$ (z -averaging). Dashed lines: $n_z = 1$ (no z -averaging). For $\Lambda = 4$ two z values thus suffice to eliminate the discretization oscillations at $n_z = 1$.

The omitted term, $\partial E_{\text{int}}^{(2)}/\partial T$, in (16) as argued above, has a negligible temperature dependence (although its magnitude is not necessarily always small compared to the terms retained). Notice that \bar{E}_{imp} is made up of a term due to the partial occupation of the local resonant level (E_{occ}), a term due to the Coulomb repulsion of electrons in this level (E_{docc}), and, a term due to the energy gained by hybridization of the local level with the conduction electrons ($E_{\text{hyb}}/2$), that is, it involves only local static correlation functions. Such quantities can be calculated very accurately and efficiently within the NRG method, within a single calculation for the total system only, a significant advantage of this approach. In some situations, the hybridization function $\Delta(\omega)$ may be strongly asymmetric and have a strong energy dependence close to $\omega = 0$. In such cases, the term $E_{\text{int}}^{(2)}$ can be calculated via the local spectral function and included in E_{imp} , which is possible within the NRG, at somewhat higher numerical cost. Another advantage of the present approach, is that discretization oscillations are far smaller for local quantities appearing in \bar{E}_{imp} than for extensive quantities, such as $\langle H \rangle$ and $\langle (H - \langle H \rangle)^2 \rangle$ appearing in the conventional approach to specific heats. Figure 3 shows the specific heat and entropy calculated with the above method, for the same parameters as in Fig. 1-2, with and without z -averaging. One sees that the discretization oscillations in the case of no z -averaging ($n_z = 1$ curves) are drastically smaller than for the corresponding $n_z = 1$ results from the conventional approach in Fig. 1. Including z -averaging makes the results of the new procedure indistinguishable from the Bethe ansatz calculations, as will be discussed in detail in Sec. IV-V.

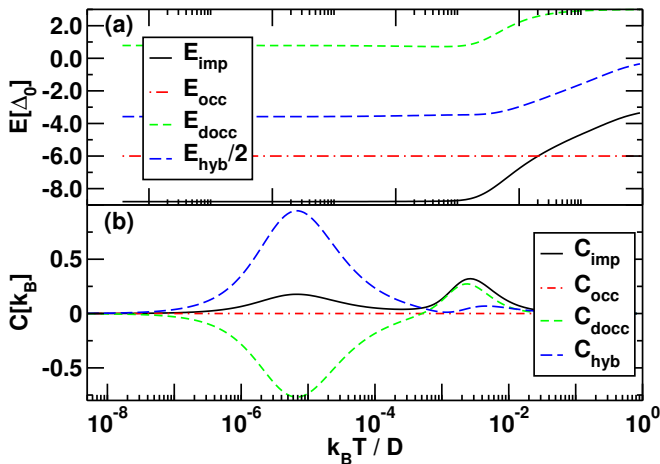


FIG. 4. (Color online) (a) The individual contributions E_{occ} , E_{docc} , and E_{hyb} to E_{imp} as a function of temperature (in units of Δ_0) for the symmetric model with parameters as in Fig. 1 (z -averaged with $n_z = 2$). (b) Temperature derivatives of the above, yielding the relative contributions C_{occ} , C_{docc} , and C_{hyb} to the specific heat C_{imp} .

In Fig. 4(a), we show the different contributions E_{occ} , E_{docc} and $E_{\text{hyb}}/2$ to the impurity internal energy for the symmetric Anderson model. Their temperature derivatives C_{occ} , C_{docc} and C_{hyb} give the relative contributions of these terms to the impurity specific heat C_{imp} and are shown in Fig. 4(b). Notice, that the Kondo induced peak in C_{imp} at low temperatures results from a delicate balance of the hybridization (C_{hyb}) and Coulomb contributions (C_{docc}), while the peak due to the resonant level at high temperatures is mainly due to the Coulomb term. The latter trend persists also for the asymmetric model, as shown in Fig. 5. Notice also that the gain in energy due to hybridization diminishes at high temperatures, reflecting the decoupling of the impurity from the conduction electrons in this limit. In general, however, the interaction of the impurity with the environment via the hybridization term provides an essential contribution at all non-zero hybridization strengths.

We now quantify the error in neglecting $\partial E_{\text{int}}^{(2)}(T)/\partial T$ in Eq. (16) for the calculation of impurity specific heats by, (a), comparing the result for C_{imp} obtained within the new method with the Bethe ansatz calculations, and, (b), explicitly calculating the contribution $\partial E_{\text{int}}^{(2)}(T)/\partial T$. Figure 6(a) shows the comparison to the Bethe ansatz calculation, where we also include the specific heat from the conventional approach. The relative deviation of the NRG calculations to the Bethe ansatz, shown in Fig. 6(b), is below 1% for all temperatures $T < 0.01 = 10\Delta_0$. For $T \ll T_K$, the relative error in C_{imp} from the internal energy is 0.1% and 0.5% in the conventional approach. The relative error exhibits remnants of the discretization oscillations, which are not completely eliminated with z -averaging. Notice also that the errors in the two NRG calculations have the same error (relative to the

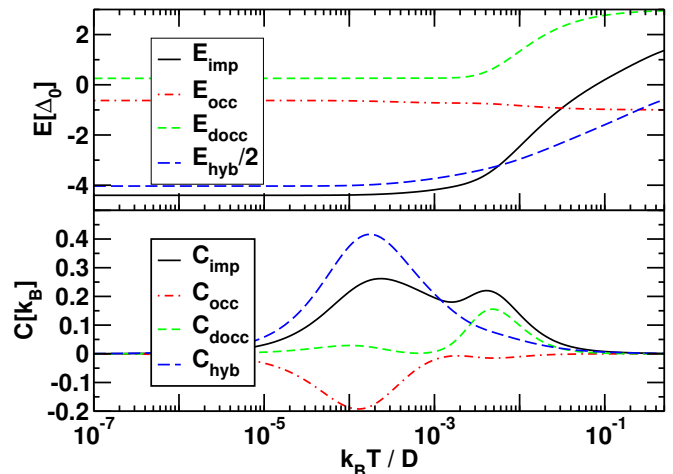


FIG. 5. (Color online) (a) The individual contributions E_{occ} , E_{docc} , and E_{hyb} to E_{imp} as a function of temperature (in units of Δ_0) for the asymmetric model with parameters as in Fig. 1, but for an asymmetric level position $\varepsilon_d/\Delta_0 = -1$ (z -averaged with $n_z = 2$). (b) Temperature derivatives of the above, yielding the relative contributions C_{occ} , C_{docc} , and C_{hyb} to the specific heat C_{imp} .

Bethe ansatz) in the high temperature limit, $T \gg \Delta_0$. Hence, the latter error is not due to neglect of $E_{\text{int}}^{(2)}$ in Eq. (15). Instead, it reflects, (a), the different high energy cut-off schemes in NRG and Bethe ansatz, and, (b), the finite size errors in the high energy excitation spectrum in NRG, since the latter stem from the shortest chains diagonalized (typically $m = 4 - 6$), which are also the ones most sensitive to the logarithmic discretization. The fact that the errors in both NRG calculations also correlate at lower temperatures ($T \lesssim \Delta_0$) suggests that the neglect of $E_{\text{int}}^{(2)}$ in Eq. (15) is not the main source of error in calculating $C_{\text{imp}}(T)$. An explicit calculation that illustrates this is shown in Fig. 7. As stated above, the value of $E_{\text{int}}^{(2)}$ is of order Δ_0/π , however, one clearly sees in Fig. 7(a) that $E_{\text{int}}^{(2)}$ has little temperature dependence (relative to the other contributions) for all temperatures extending up to the bandwidth $D = 1$. Its relative contribution to the impurity specific heat, shown in Fig. 7(b), for an energy dependent $\Delta(\omega)$, is negligible, typically contributing below 0.5%.

IV. RESULTS FOR THE SYMMETRIC MODEL

In this section we show results for the entropy and specific heat of the Anderson model at the particle-hole symmetric point $\varepsilon_d = -U/2$. Results for zero magnetic field and increasing correlation strength U/Δ_0 are presented in Sec. (IV A) and results for finite magnetic fields are given in Sec. (IV B).

The symmetric Anderson model has been investigated in detail¹ and is well understood. For $U/\Delta_0 \gg 1$ and

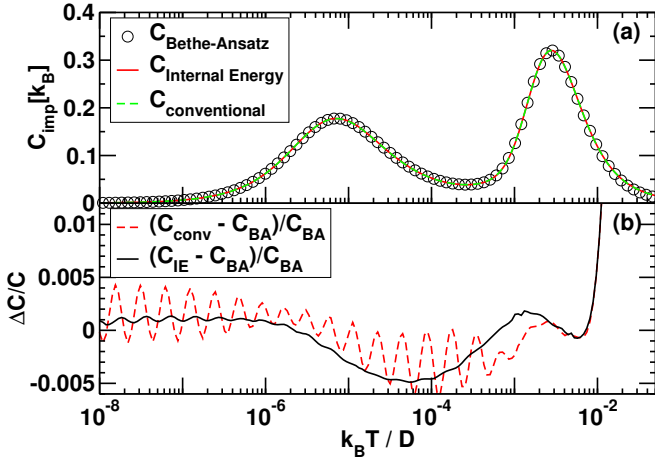


FIG. 6. (Color online) (a) Comparison of specific heat, $C_{\text{imp}}(T)$, from the impurity internal energy (solid line) and conventional approach (dashed line) with the Bethe ansatz calculation (symbols) for the symmetric Anderson model with parameters as in Fig. 1. NRG parameters also as in Fig. 1 with $n_z = 2$. (b) The relative deviation with respect to the Bethe ansatz result of the new (solid line) and conventional (dashed line) approaches.

$-\varepsilon_d \gg \Delta_0$, a local spin $S = 1/2$ magnetic moment forms on the impurity. In this limit, the physics of the symmetric model at low temperatures $T \ll \min(|\varepsilon_d + U|, |\varepsilon_d|, D)$ is that of the Kondo model

$$H_K = H_0 + J \mathbf{S} \cdot \mathbf{s}_0, \quad (18)$$

where, J is an antiferromagnetic exchange coupling between the local spin S and the conduction electron spin-density \mathbf{s}_0 at the impurity site. The value of J is given by the Schrieffer-Wolff transformation⁵⁶ $J = 4V^2/U$. The low temperature properties (for $U \gg \Delta_0$) are universal functions of T/T_K and B/T_K where we choose to define the Kondo scale from the Bethe ansatz result for the $T = 0$ susceptibility $\chi(0)$ via $\chi(0) = (g\mu_B)^2/4T_K$. For $U \gg \Delta_0$, T_K is given by

$$T_K = \sqrt{U\Delta_0/2} e^{-\pi U/8\Delta_0 + \pi\Delta_0/2U}, \quad (19)$$

within corrections which are exponentially small in $U/\pi\Delta_0$ (see Ref. 1). For $U = 0$, the symmetric Anderson model reduces to a resonant level model and the relevant low temperature scale is then Δ_0 .

A. Zero magnetic field

A comparison of the new approach with Bethe ansatz calculations is shown in Fig. 8 for the temperature dependence of the impurity specific heat and entropy for increasing values of the Coulomb interaction U/Δ_0 . For $U/\Delta_0 = 12$, the Kondo induced peak in the specific heat at $T_p = \alpha T_K$ with $\alpha \approx 0.29$ is well separated from the

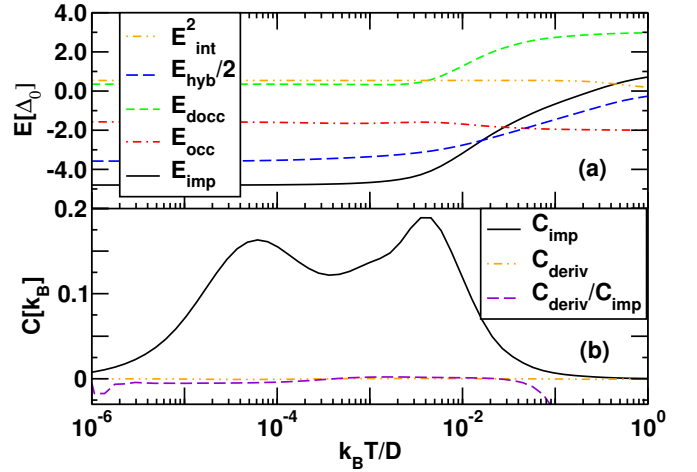


FIG. 7. (Color online) (a) The contribution $E_{\text{int}}^{(2)}$ to E_{imp} as a function of temperature compared with E_{occ} , E_{docc} and E_{hyb} (in units of Δ_0) for the asymmetric model. Model parameters: $U = 12\Delta_0$, $\Delta_0 = 0.001D$, $\varepsilon_d/\Delta_0 = -2$ with a semi-elliptic hybridization function $\text{Im}[\Delta(\omega)] = -\frac{\Delta_0}{D} \sqrt{(D^2 - \omega^2)}$. A small $\Lambda = 1.5$ was used, which allows the spectral function entering $E_{\text{int}}^{(2)}$ to be obtained without z -averaging. (b) The contribution $C_{\text{deriv}} = \partial E_{\text{int}}^{(2)}/\partial T$ to C_{imp} . The relative size of C_{deriv} to C_{imp} lies between 0.2% and 0.5% for all temperatures, except at temperatures approaching the bandwidth $D = 1$.

peak at $T \approx |\varepsilon_d|$ due to the resonant level. With decreasing U/Δ_0 , the Kondo effect is suppressed and the Kondo induced peak in $C(T)$ eventually merges with the peak due to the resonant level for $U/\Delta_0 \rightarrow 0$. Good agreement between the NRG and the exact Bethe ansatz calculations is seen for all values of U/Δ_0 .

B. Finite magnetic field

At finite magnetic fields $B > 0$, the $SU(2)$ spin symmetry which we use in the NRG calculations, is broken. Therefore, in order to carry out calculations at finite magnetic field $B > 0$, preserving the numerical advantages of the full $SU(2)$ symmetry, such as the increased number of states that can be retained, we obtained the finite field results by mapping the symmetric positive U Anderson model onto the negative- U Anderson model in the absence of a magnetic field but with local level given by $\varepsilon_d = -U/2 - B/2$ with U negative.^{57,58} This correspondence results from a particle-hole transformation on the down spins only: $d_{\downarrow} \rightarrow d_{\downarrow}^{\dagger}$, $d_{\uparrow} \rightarrow d_{\uparrow}$, and $c_{k\downarrow} \rightarrow c_{-k\downarrow}^{\dagger}$, $c_{k\uparrow} \rightarrow c_{k\uparrow}$ with a particle-hole symmetric band $\epsilon_k = -\epsilon_{-k}$.

Figure 9 shows the temperature dependence of $C_{\text{imp}}(T, B)$ for $B/T_K \geq 1$ using our new approach and compared with Bethe ansatz calculations. The Kondo peak in the specific heat shifts to higher fields with increasing B and its position scales as B^2/T_K for $T_K \ll$

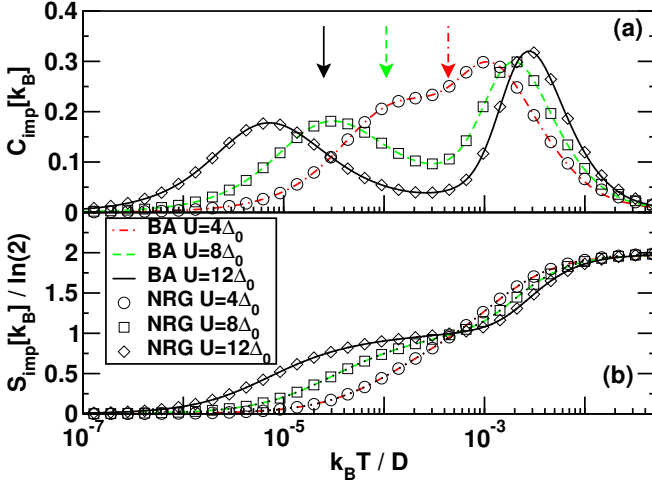


FIG. 8. (Color online) Temperature dependence of, (a), the impurity specific heat, $C_{\text{imp}}(T)$, and, (b), the impurity entropy, $S_{\text{imp}}(T)/\ln(2)$, for the symmetric Anderson model with $\Delta_0 = 0.001D$ and increasing values of the Coulomb interaction: $U/\Delta_0 = 4, 8, 12$. Arrows in (a) indicated the Kondo scale T_K defined in Eq. 19. Symbols: new approach using NRG with $\Lambda = 4$ with an energy cut-off $e_c(\Lambda = 4) = 40$, and z -averaging [$n_z = 2$, $z = 1/4, 3/4$]. Lines: corresponding Bethe ansatz calculations.

$B \ll \varepsilon_d$. In contrast, the resonant level peak remains approximately fixed at $T \approx \varepsilon_d$. As B approaches the value ε_d , the two peaks merge into one peak at $T \approx \varepsilon_d$, with approximately twice the height of the $B = 0$ resonant level peak, and containing the whole entropy $S_{\text{imp}}/k_B = \ln(4)$. The low field behaviour of $C_{\text{imp}}(T, B)$, also compared to Bethe ansatz calculations, is shown in Fig. 9(a) as $T_K \gamma(T, B) = C_{\text{imp}}(T, B)/(T/T_K)$ versus T/T_K for $B/T_K \leq 2$. For $T, B \rightarrow 0$, $\gamma(T, B) \rightarrow \gamma(0, 0) \sim 1/T_K$ where $\gamma(0, 0)$ is the linear coefficient of specific heat. This is strongly enhanced for $U/\Delta_0 \gg 1$ due to the exponential decrease of T_K . A finite magnetic field of order T_K significantly suppresses the Kondo effect and results in smaller values of $\gamma(0, B)$. As another check on the accuracy of our calculations, we estimate the Wilson ratio $R_W = 4\pi^2\chi(0)/3\gamma(0, 0)$. This takes the value 2 in the Kondo regime of the symmetric Kondo model (i.e., for $U \gg \Delta_0$). From the definition of T_K , we have that the susceptibility $\chi(0) = 1/4T_K$, and from Fig. 9(a) we extract $\gamma(0, 0) \approx 1.64/T_K$, resulting in $R_W \approx 2.006$, that is, a relative error in R_W below 1%.

V. RESULTS FOR THE ASYMMETRIC MODEL

Figure 10 shows the impurity specific heat versus temperature for the asymmetric Anderson model, that is, for $\varepsilon_d > -U/2$, calculated within the new approach. For comparison, we also show the corresponding Bethe ansatz calculations. One sees again excellent agreement at all temperatures between the two methods. Results for

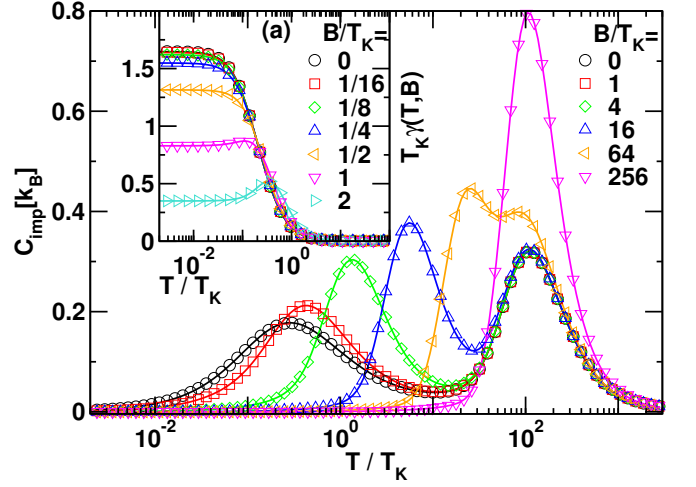


FIG. 9. (Color online) Temperature dependence of the impurity specific heat, $C_{\text{imp}}(T, B)$, for the symmetric Anderson model for $U/\Delta_0 = 12$, $\Delta_0 = 0.001D$ and increasing values of the magnetic field $B/T_K \geq 1$ where the Kondo scale T is defined in Eq. 19. Symbols: NRG calculations $\Lambda = 4$ with an energy cut-off $e_c(\Lambda = 4) = 40$, and z -averaging [$n_z = 2$, $z = 1/4, 3/4$]. Lines: Bethe ansatz calculations. Inset (a): $T_K \gamma(T, B)$ versus T/T_K for several values of $B/T_K \leq 2$, where $\gamma(T, B) = C_{\text{imp}}(T, B)/T$.

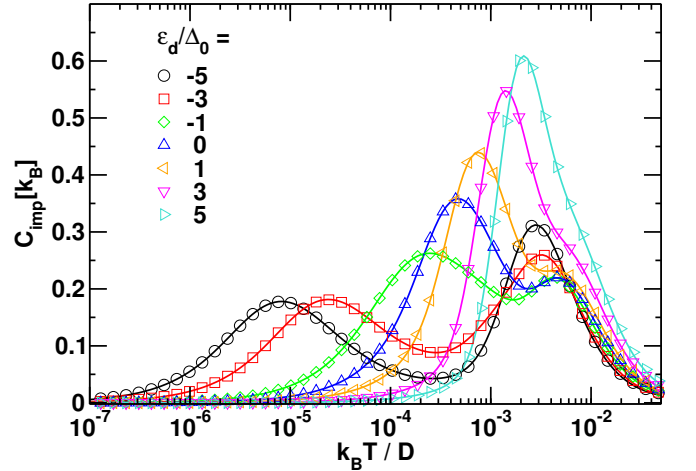


FIG. 10. (Color online) Temperature dependence of $C_{\text{imp}}(T)$ for $U/\Delta_0 = 12$, $\Delta_0 = 0.001D$ and local level positions ε_d/Δ_0 ranging from Kondo ($\varepsilon_d/\Delta_0 \leq -1$), mixed valence ($|\varepsilon_d/\Delta_0| \leq 1$), and empty orbital ($\varepsilon_d/\Delta_0 > 1$) regimes. Symbols: NRG calculations (new approach, z -averaging and NRG parameters as in Fig. 1). Lines: Bethe ansatz calculations.

$\varepsilon_d < -U/2$ are not shown, since these can be obtained from results for $\varepsilon_d > -U/2$ by noting that the Anderson model with parameters ε_d, U, V transforms, under a particle-hole transformation applied to both spin species, to an Anderson model with parameters $-(\varepsilon_d + U), U, V$. This holds for a particle-hole symmetric constant density of states, the case considered here.

The specific heat curves for the asymmetric model are

more complicated than those of the symmetric model. In the latter, the relevant excitations were the low temperature spin flip excitations, characterized by the Kondo scale T_K , and the excitations involving addition or removal of an electron from the resonant level, both characterized by an energy $|\varepsilon_d| = U/2$. This accounts for the two peaks in the specific heat of the symmetric model: A high temperature peak at $T \approx |\varepsilon_d|$ and a low temperature Kondo induced peak at $T \approx T_K$. For the asymmetric Anderson model, three types of excitation are possible: Low-temperature spin flip excitations, associated with the Kondo scale $T_L = \sqrt{U\Delta_0/2}e^{-\pi|\varepsilon_d|/|U/2|}$ of the asymmetric model,¹ and excitations associated with, (i), removing an electron from a singly occupied level (with energy scale $|\varepsilon_d|$) and (ii), removing an electron from a doubly occupied level (with energy scale $|\varepsilon_d + U|$). Thus, three peaks can be present in $C_{\text{imp}}(T)$: a Kondo induced peak at $T \approx T_L$, and two charge fluctuation induced peaks at $T \approx T_1 = |\varepsilon_d|$ and $T \approx T_2 = |\varepsilon_d + U|$, respectively. In Fig. 10, the two high temperature peaks are seen in the mixed valence regime and partly also in the empty orbital regime (where the upper peak at T_2 appears as a shoulder of the main peak at T_1). However, in the Kondo regime, the cases $\varepsilon_d/\Delta_0 = -5, -3$ with the choice $U = 12\Delta_0$ result in $T_1/\Delta_0 = 5, 3$ and $T_2/\Delta_0 = 7, 9$. In these cases, T_1 and T_2 are too close for separate peaks to be seen. In order to clarify this, we carried out calculations for $U = 48\Delta_0 \gg \Delta_0$, and $\varepsilon_d/\Delta_0 = -10, -8, -6, -4, -2$ in the Kondo regime, for which $T_1/\Delta_0 = 10, 8, 6, 4, 2$ and $T_2/\Delta_0 = 38, 40, 42, 44, 46 \gg T_1/\Delta_0$ are disparate scales. Figure 11 shows how the peaks at $T \approx T_1$ and $T \approx T_2$ evolve from the peak at $T \approx |\varepsilon_d| = U/2$ of the symmetric model (dashed line in Fig. 11) on increasing ε_d above $-U/2$. Simultaneously, the Kondo peak in the specific heat at T_L shifts to higher temperatures and eventually merges with the peak at T_1 when the mixed valence regime is reached (i.e., for $\varepsilon_d = -\Delta_0$). Thereafter, only the high temperature peaks at T_1 and T_2 are present. Notice also, that in the mixed valence regime T_1 differs significantly from $|\varepsilon_d|$, a result of non-trivial renormalizations present in the mixed valence regime, but absent in the empty orbital regime.

VI. GENERALIZATION TO OTHER MODELS

The approach of Sec. III can be straightforwardly generalized to multiorbital and multichannel Anderson impurity models with arbitrary local Coulomb interactions, as we briefly outline in Sec. VIA. In addition, in Sec. VIB we discuss its application to dissipative two state systems and the anisotropic Kondo model (AKM).

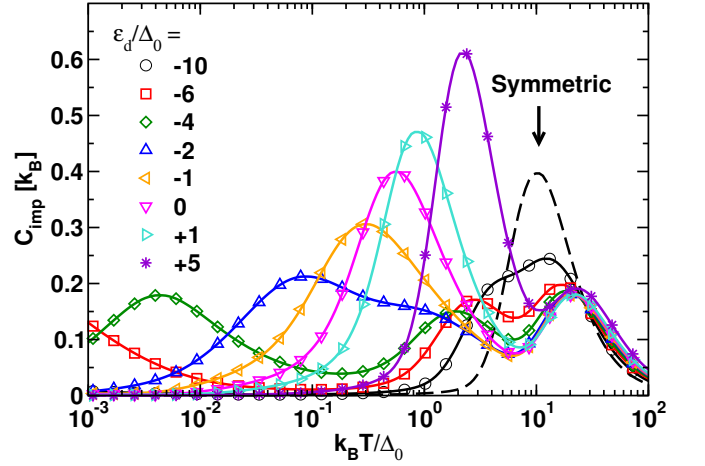


FIG. 11. (Color online) Temperature dependence of $C_{\text{imp}}(T)$ for $U/\Delta_0 = 48$, $\Delta_0 = 0.0001D$ and local level positions $\varepsilon_d/\Delta_0 = -10, -6, -4, -2$ (Kondo regime), $\varepsilon_d/\Delta_0 = -1, 0, +1$ (mixed valence regime) and $\varepsilon_d/\Delta_0 = +5$ (empty orbital regime). NRG using the new approach (symbols) and conventional approach (solid lines) [$\Lambda = 20, n_z = 4, e_c(\Lambda) = 130$]. Dashed line: resonant level peak in C_{imp} at $T/\Delta_0 \approx |\varepsilon_d|/\Delta_0 = U/2\Delta_0 = 24$ for the symmetric model (the Kondo induced peak at much lower T is not shown). The two high temperature peaks of the asymmetric model evolve from this peak when the asymmetry is finite.

A. Multiorbital and multichannel Anderson models

The multiorbital and multichannel Anderson impurity model is given by $H = H_{\text{imp}} + H_0 + H_{\text{int}}$, where $H_{\text{imp}} = \sum_{\alpha\sigma} \varepsilon_\alpha d_{\alpha\sigma}^\dagger d_{\alpha\sigma} + H_C(U, U', J)$, describes the impurity with a set of local levels having energies $\varepsilon_{d\alpha}$, $\alpha = 1, \dots, g$ and $H_C(U, U', J)$ is the local Coulomb interaction involving intra-orbital U , inter-orbital U' and a Hund's exchange term J . The conduction electrons are described by $H_0 = \sum_{k\alpha\sigma} \epsilon_{k\alpha} c_{k\alpha\sigma}^\dagger c_{k\alpha\sigma}$ where $\epsilon_{k\alpha}$ is the kinetic energy of electrons in band α . These bands hybridize with hybridization strengths V_α , $\alpha = 1, \dots, g$ to the local levels via $H_{\text{int}} = \sum_{k\alpha\sigma} V_\alpha (c_{k\alpha\sigma}^\dagger d_{\alpha\sigma} + d_{\alpha\sigma}^\dagger c_{k\alpha\sigma})$. Let $\Delta_\alpha(\omega) = \sum_k V_\alpha^2 / (\omega - \epsilon_{k\alpha})$ denote the hybridization functions characterizing H_{int} . Proceeding as in Sec. III, we write the impurity internal energy as $E_{\text{imp}} = E_{\text{total}} - E_0$ where $E_{\text{total}} = \langle H \rangle$ is the total energy and $E_0 = \langle H_0 \rangle = \sum_{k\alpha\sigma} \epsilon_{k\alpha} \langle c_{k\alpha\sigma}^\dagger c_{k\alpha\sigma} \rangle_0$ is the energy of the non-interacting conduction electrons in the absence of the impurity. The latter is given by $E_0 = \sum_{\alpha\sigma} \int d\epsilon f(\epsilon) \epsilon N_\alpha(\epsilon)$, where $f(\epsilon)$ is the Fermi function and $N_\alpha(\epsilon) = \sum_k \delta(\epsilon - \epsilon_{k\alpha})$ is the non-interacting conduction electron density of states per spin for band α . E_{total} is a sum of local occupation number contributions $E_{\text{occ}} = \sum_{\alpha\sigma} \varepsilon_\alpha \langle n_{\alpha\sigma} \rangle$ and local Coulomb terms $E_C = \langle H_C(U, U', J) \rangle$ and two further terms involving the interacting band $E_{\text{cond}} = \sum_{k\alpha\sigma} \epsilon_{k\alpha} \langle c_{k\alpha\sigma}^\dagger c_{k\alpha\sigma} \rangle$ and the hybridization energy $E_{\text{hyb}} = \sum_{\alpha\sigma} V_\alpha \langle d_{\alpha\sigma}^\dagger f_{0\alpha\sigma} + \text{H.c.} \rangle$ where $V_\alpha f_{0\alpha\sigma} = \sum_k c_{k\alpha\sigma}$:

$$E_{\text{total}} = E_{\text{occ}} + E_C + E_{\text{cond}} + E_{\text{hyb}}. \quad (20)$$

We evaluate the latter two contributions as in Sec. III, finding

$$E_{\text{hyb}} = -\frac{2}{\pi} \sum_{\alpha\sigma} \int d\omega f(\omega) \text{Im} [G_{d\alpha\sigma}(\omega) \Delta_\alpha(\omega)], \quad (21)$$

and $E_{\text{cond}} = E_0 + E_{\text{int}}$, where

$$E_{\text{int}} = \frac{1}{\pi} \sum_{\alpha\sigma} \int d\omega f(\omega) \text{Im} \left[G_{d\alpha\sigma}(\omega) \frac{\partial}{\partial \omega} (\omega \Delta_\alpha(\omega)) \right] \\ = E_{\text{int}}^{(1)} + E_{\text{int}}^{(2)}, \quad (22)$$

$$E_{\text{int}}^{(1)} = \frac{1}{\pi} \sum_{\alpha\sigma} \int d\omega f(\omega) \text{Im} [G_{d\alpha\sigma}(\omega) \Delta_\alpha(\omega)] \quad (23)$$

$$E_{\text{int}}^{(2)} = \frac{1}{\pi} \sum_{\alpha\sigma} \int d\omega f(\omega) \text{Im} \left[G_{d\alpha\sigma}(\omega) \omega \frac{\partial \Delta_\alpha(\omega)}{\partial \omega} \right], \quad (24)$$

and $G_{d\alpha\sigma}(\omega)$ is the retarded Green function for local level α . Combining $E_{\text{int}}^{(1)}$ with E_{hyb} gives for the impurity internal energy

$$E_{\text{imp}} = E_{\text{occ}} + E_C + \frac{1}{2} E_{\text{hyb}} + E_{\text{int}}^{(2)}, \quad (25)$$

where, as before, all contributions except the last one are evaluated as local static correlation functions. For reasons discussed in Sec. III, the temperature dependence of the last term is negligible in many cases and the impurity specific heat can be calculated to high accuracy via

$$C_{\text{imp}} = \frac{\partial E_{\text{occ}}}{\partial T} + \frac{\partial E_C}{\partial T} + \frac{1}{2} \frac{\partial E_{\text{hyb}}}{\partial T} \quad (26)$$

$$= \frac{\partial E_{\text{ionic}}}{\partial T} + \frac{1}{2} \frac{\partial E_{\text{hyb}}}{\partial T}, \quad (27)$$

where $E_{\text{ionic}} = \langle H_{\text{imp}} \rangle$.

B. Dissipative two state systems and the anisotropic Kondo model

The method of Sec. III can be applied to bosonic models such as the dissipative two state system,^{4,5} and for Ohmic dissipation, one can further relate the results to the AKM and related models (for example, a two-level system in a metallic environment⁵⁹). Dissipative two state systems are of interest in many contexts, including the description of qubits coupled to their environment.

The Hamiltonian of the dissipative two state system is given by $H = H_S + H_B + H_I$. The first term $H_S = -\frac{1}{2} \Delta_0 \sigma_x + \frac{1}{2} \epsilon \sigma_z$ describes a two-level system with bias splitting ϵ and tunneling amplitude Δ_0 , and $\sigma_{i=x,y,z}$ are Pauli spin matrices. $H_B = \sum_i \omega_i (a_i^\dagger a_i + 1/2)$ is the environment and consists of an infinite set of harmonic oscillators ($i = 1, 2, \dots, \infty$) with $a_i (a_i^\dagger)$ the annihilation (creation) operators for a harmonic oscillator of frequency ω_i and $0 \leq \omega_i \leq \omega_c$, where ω_c is an upper cut-off frequency. The non-interacting density of states of the environment is denoted by $g(\omega) = \sum_i \delta(\omega - \omega_i)$ and

is finite in the interval $[0, \omega_c]$ and zero otherwise. Finally, $H_I = \frac{1}{2} \sigma_z \sum_i \lambda_i (a_i + a_i^\dagger)$ describes the coupling of the two-state system co-ordinate σ_z to the oscillators, with λ_i denoting the coupling strength to oscillator i . The function $\Gamma(\omega + i\delta) = \sum_i (\lambda_i/2)^2 / (\omega - \omega_i + i\delta) = \int d\omega' (\lambda(\omega')/2)^2 g(\omega') / (\omega - \omega' + i\delta)$ characterizes the system-environment interaction. The Ohmic two state system, specified by a spectral function $J(\omega) = -\frac{1}{\pi} \text{Im} \Gamma(\omega + i\delta) \sim \alpha \omega$ for $\omega \rightarrow 0$, where α is the dimensionless dissipation strength, is equivalent to the AKM $H = \sum_{k\sigma} \epsilon_k c_{k\sigma}^\dagger c_{k\sigma} + \frac{J_\perp}{2} (S^+ s_0^- + S^- s_0^+) + J_\parallel S_z s_0^z + B S_z$, where J_\perp (J_\parallel) is the transverse (longitudinal) part of the Kondo exchange interaction and B is a local magnetic field. The correspondence is given by $\rho J_\perp = -\Delta_0/\omega_c$ and $\alpha = (1 + 2\delta/\pi)^2$ where $\delta = \arctan(-\pi \rho J_\parallel/4)$ and ρ is the density of states of the conduction electrons in the AKM.^{4,5,60-62} The low energy scale of the Ohmic two state system is the renormalized tunneling amplitude Δ_r given by $\Delta_r/\omega_c = (\Delta_0/\omega_c)^{1/(1-\alpha)}$ and corresponds to the low energy Kondo scale T_K of the AKM. Special care is needed to obtain results for the Ohmic two state system from the AKM in the vicinity of the singular point $\alpha \rightarrow 1^-$, since this corresponds to $J_\parallel \rightarrow 0$ but with the condition $0 < J_\perp < J_\parallel$, that is, in terms of parameters of the Ohmic two state system one requires $\Delta_0/\omega_c \ll 1 - \alpha \ll 1$ in order to investigate the vicinity of $\alpha = 1$ within the AKM.⁵

The specific heat, $C_{\text{imp}} = \partial E_{\text{imp}}/\partial T$, of the Ohmic two-state system is defined via an impurity internal energy $E_{\text{imp}} = E_{\text{total}} - E_0$, where $E_{\text{total}} = \langle H \rangle = \langle H_S \rangle + \langle H_B \rangle + \langle H_I \rangle$ and $E_0 = \langle H_B \rangle_0 = \sum_i \omega_i \langle a_i^\dagger a_i \rangle_0 + E_{\text{zp}} = \int_0^{\omega_c} d\omega \omega n(\omega) g(\omega) + E_{\text{zp}}$ where $n(\omega) = 1/(e^{\beta\omega} - 1)$ is the Bose distribution function and the zero point energy E_{zp} can be dropped, as it cancels in the difference $\langle H_B \rangle - E_0 = E_B - E_0$ appearing in E_{imp} . Evaluating $E_B - E_0$ and $E_I = \langle H_I \rangle$ following the approach in Sec. III, we find

$$E_B - E_0 = \frac{1}{\pi} \int d\omega n(\omega) \text{Im} \left[\chi_{zz}(\omega + i\delta) \frac{\partial}{\partial \omega} (\omega \Gamma(\omega + i\delta)) \right] \\ = E_B^{(1)} + E_B^{(2)}, \quad (28)$$

$$E_B^{(1)} = \frac{1}{\pi} \int d\omega n(\omega) \text{Im} [\chi_{zz}(\omega + i\delta) \Gamma(\omega + i\delta)] \quad (29)$$

$$E_B^{(2)} = \frac{1}{\pi} \int d\omega n(\omega) \text{Im} \left[\chi_{zz}(\omega + i\delta) \omega \frac{\partial \Gamma(\omega + i\delta)}{\partial \omega} \right] \quad (30)$$

and

$$E_I = -\frac{1}{\pi} \int d\omega n(\omega) \text{Im} [\chi_{zz}(\omega + i\delta) \Gamma(\omega + i\delta)], \quad (31) \\ (32)$$

where $\chi_{zz}(\omega + i\delta) = \langle \langle \sigma_z; \sigma_z \rangle \rangle_{\omega+i\delta}$ is the longitudinal retarded dynamic susceptibility and $\Gamma(\omega + i\delta)$, characterizing the system-environment interaction, was defined above. Noting that $E_B^{(1)}$ exactly cancels E_I in the impurity internal energy, we find

$$E_{\text{imp}} = -\frac{1}{2} \Delta_0 \langle \sigma_x \rangle + \frac{1}{2} \epsilon \langle \sigma_z \rangle + E_B^{(2)}, \quad (33)$$

that is, $E_{\text{imp}} = E_S + E_B^{(2)}$. The term $E_B^{(2)}$ gives a non-negligible contribution to the impurity internal energy. For example, in the Ohmic case with spectral function $J(\omega) = -\frac{1}{\pi} \text{Im}\Gamma(\omega + i\delta) \sim \alpha\omega$ we have $\omega \partial J(\omega)/\partial \omega \sim \alpha\omega$ at low frequencies, so $E_B^{(2)}$ provides a contribution proportional to α . By carrying out specific heat calculations on the AKM, we find numerically that the impurity specific heat is consistent with setting $E_B^{(2)} = \frac{1}{2}\alpha\Delta_0\langle\sigma_x\rangle + A$, with A being a weakly temperature dependent term, and negligible for calculating the specific heat, except in the limit $\alpha \rightarrow 1^-$. The latter limit is difficult to treat numerically because of the vanishing low energy scale Δ_r for $\alpha \rightarrow 1^-$ (e.g., for $\Delta_0/\omega_c = 0.01$ and $\alpha = 0.9$ we have $\Delta_r/\omega_c = 10^{-20}$). Hence, except in this extreme limit, and as we show below by comparing with exact results, the impurity specific heat can be obtained accurately from $C_{\text{imp}} = \frac{\partial E_{\text{imp}}}{\partial T}$ by using

$$E_{\text{imp}} \approx -\frac{1}{2}\Delta_0(1-\alpha)\langle\sigma_x\rangle + \frac{1}{2}\epsilon\langle\sigma_z\rangle. \quad (34)$$

Figure 12 shows results obtained in this way for $C_{\text{imp}}(T)/(k_B T/\Delta_r)$ compared to Bethe ansatz calculations for the AKM⁶³ for a range of dissipation strengths. These results recover the known results for asymptotically high and low temperatures.⁶⁴ In common with specific heats of other correlated electron systems as a function of interaction strength,⁶⁵ we observe a crossing point in $C(T)/T$ (here, at $k_B T/\Delta_r \approx 0.67$). On decreasing the dissipation strength from strong ($\alpha > 1/2$) to weak values ($\alpha < 1/2$) the T^3 coefficient of the specific heat changes sign for $\alpha < 1/3$ resulting in the appearance of a finite temperature peak in $C(T)/T$. This is shown in more detail in Fig. 13. It signifies the development of a gap $\sim \Delta_0$ in the spectrum as $\alpha \rightarrow 0$. For $\alpha = 0$ one eventually recovers the Schottky specific heat for a non-interacting two level system. The expression (34) for the Ohmic two system is also the impurity internal energy of the equivalent AKM (indeed, the NRG results that we showed were for this model). The correspondence of model parameters was given above and the operators σ_x and σ_z are identified, under bosonization,^{4,5,60,62} with the spin-flip operator $S^+s_0^- + S^-s_0^+$ and the local S_z in the AKM, respectively. The zero temperature expectation values $\langle\sigma_x\rangle$ and $\langle\sigma_z\rangle$ (and the associated entanglement entropy of the qubit) have been studied previously as a function of dissipation strength and finite bias.^{66,67}

We expect that the term $E_B^{(2)}$ is non-negligible also for generic spectral functions $J(\omega) \sim \omega^s$ and certainly for the sub-Ohmic case $s < 1$. Recent results for the local spin dynamics of the sub-Ohmic spin boson model⁶⁸ could shed light on this.

The result (34) shows that a significant contribution to the impurity internal energy and specific heat arises from the (interacting) bath contribution $E_B^{(2)}$, which remains finite for arbitrarily small α . Thus, while a definition of the internal energy of the system via $E_S = \langle H_S \rangle$ and the specific heat via $C_S = \partial E_S/\partial T$, might seem reason-

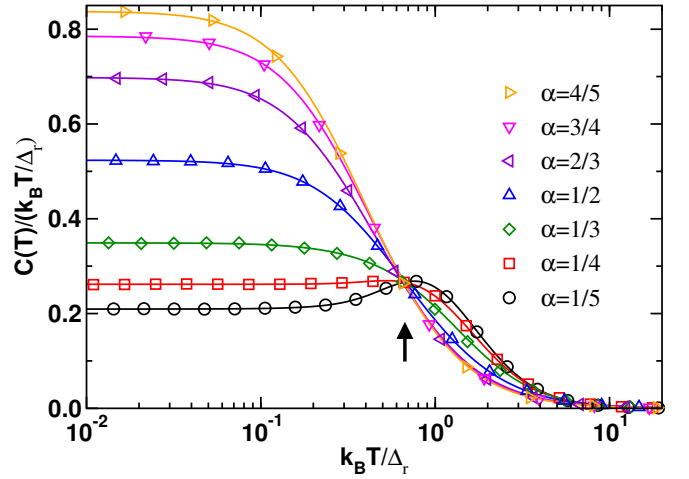


FIG. 12. (Color online) Specific heat, $C_{\text{imp}}(T)/k_B T/\Delta_r$, of the Ohmic two state system as a function of reduced temperature $k_B T/\Delta_r$, for a range of dissipation strengths $\alpha = 1/5, 1/4, 1/3, 1/2, 2/3, 3/4, 4/5$. Symbols: NRG results in new approach. Lines: Bethe ansatz results. The renormalized tunneling amplitude Δ_r from the Bethe ansatz is used. The vertical arrow indicates the approximate crossing point at $k_B T/\Delta_r \approx 0.67$. Model parameters: $\Delta_0/\omega_c = 0.005$. NRG parameters: $\Lambda = 10, n_z = 4$ retaining 860 states per NRG iteration.

able for a small quantum system *weakly* coupled to an infinite bath, such a definition yields, in general, a specific heat C_S which differs from C_{imp} .^{69–72} One system for which the two definitions agree is the harmonic oscillator coupled Ohmically to an infinite bath of harmonic oscillators.⁶⁹ This result, however, represents a special case, and, moreover, is sensitive to details of the cut-off scheme used for the spectral function $J(\omega)$ (see Ref. 69 and 72). The use of E_{imp} and C_{imp} as definitions for the system internal energy and specific heat in the context of open quantum systems^{5,73} also provides an unambiguous prescription for their measurement in terms of two separate measurements,^{71,74} one for H and one for H_0 .

We note also that the impurity specific heat $C_{\text{imp}}(T) = C(T) - C_0(T)$ need not be positive at all temperatures and only the positivity of $C(T)$ and $C_0(T)$ in Eqs. (1) and (2) is guaranteed by thermodynamic stability of the equilibrium systems described by H and H_0 (see Ref. 75). Examples of systems where the difference, $C_{\text{imp}}(T)$, may be negative in some temperature range, include quantum impurities exhibiting a flow between a stable and an unstable fixed point,⁷⁶ and magnetic impurities in superconductors.⁷⁷

VII. DISCUSSION AND CONCLUSIONS

In this paper, we introduced a new approach to the calculation of impurity internal energies and specific heats of quantum impurity models within the NRG method. For general Anderson impurity models, the impurity con-

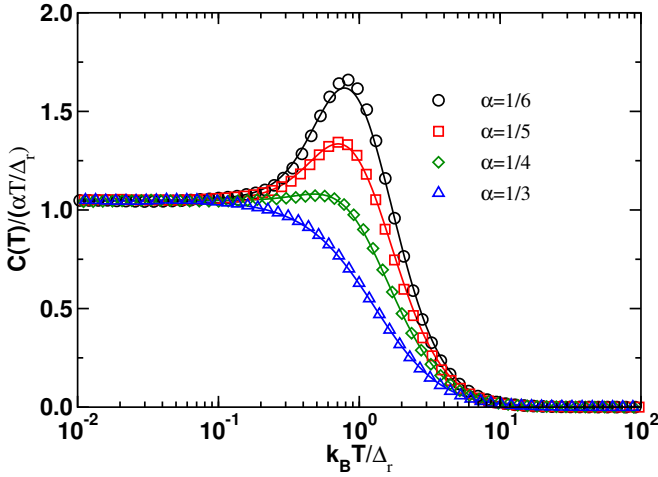


FIG. 13. (*Color online*) Specific heat, $C_{\text{imp}}(T)/(\alpha k_B T/\Delta_r)$, of the Ohmic two state system as a function of reduced temperature $k_B T/\Delta_r$, for a range of dissipation strengths $\alpha < 1/2$. Symbols: NRG results in new approach. Lines: Bethe ansatz results. In the low temperature Fermi liquid regime, $T \ll \Delta_r$, we have $C_{\text{imp}}(T)/(\alpha k_B T/\Delta_r) = \tilde{\gamma} + \tilde{\beta}(T/\Delta_r)^2$, with $\tilde{\gamma} = \pi/3$ and the T^3 coefficient in $C(T)$ changes sign for $\alpha < 1/3$ (see Ref. 62). Model parameters: $\Delta_0/\omega_c = 0.005$. NRG parameters: $\Lambda = 10, n_z = 4$ retaining 860 states per NRG iteration.

tribution to the internal energy was expressed in terms of local quantities and the main contribution to the impurity specific heat was shown to arise from local static correlation functions. For this class of models, the impurity specific heat can be obtained essentially exactly as $C_{\text{imp}}(T) = \frac{\partial E_{\text{ionic}}}{\partial T} + \frac{1}{2} \frac{\partial E_{\text{hyb}}}{\partial T}$, where $E_{\text{ionic}} = \langle H_{\text{imp}} \rangle$ and E_{hyb} is the hybridization energy. A comparison with exact Bethe ansatz calculations showed that the results for specific heats of the Anderson impurity model are recovered accurately over the whole temperature and magnetic field range. The new method has several advantages over the conventional approach to specific heats within the NRG, namely, (i), only diagonalization of the total system is required, (ii), only local quantities are required, and, (iii), discretization oscillations at large Λ are significantly smaller than in the conventional approach.

For the dissipative two state system we obtain the specific heat as $C_{\text{imp}}(T) \equiv \frac{\partial E_{\text{imp}}}{\partial T} = \frac{\partial E_S}{\partial T} + \frac{\partial E_B^{(2)}}{\partial T}$, where $E_S = \langle H_S \rangle$ is analogous to E_{ionic} in the Anderson model, and $E_B^{(2)}$ is a contribution to the energy of the system arising from the interaction with the bath. It depends on the local dynamical susceptibility and the type of coupling to the environment. For the Ohmic case, we used the equivalence of the Ohmic two state system to the AKM to show numerically that $E_B^{(2)} = \frac{1}{2} \alpha \Delta_0 \langle \sigma_x \rangle + A$ with A having a negligible temperature dependence, except in the extreme limit $\alpha \rightarrow 1^-$. Comparison with exact Bethe ansatz calculations on the AKM confirmed the above.

The approach described in this paper applies to en-

ergy dependent hybridizations also, see Fig. 7, so, inclusion of the term $E_{\text{int}}^{(2)}$ in Eq. (15), could prove useful in applications to quantum impurities with a pseudogap density of states.^{37,78} It may also be applied within other methods for solving quantum impurity models, for example, within continuous time⁷⁹ or Hirsch-Fey⁸⁰ quantum Monte Carlo techniques or exact diagonalization methods (for a recent review see Ref. 81 and references therein). Local static correlation functions, such as the double occupancy, required for E_{imp} , are readily extracted within these approaches.⁸²

Within a DMFT treatment of correlated lattice models,^{19–22} the hybridization function Δ acquires an important temperature and frequency dependence $\Delta(\omega) \rightarrow \Delta(\omega, T)$. The latter enters explicitly in the term $E_{\text{int}}^{(2)}$, whose inclusion could offer an approach to the calculation of specific heats of correlated lattice models. The thermodynamic potential of the latter⁸³ is a sum of two parts, one depending on the local self-energy, which is the central quantity calculated in DMFT, and another equal to the thermodynamic potential, $\Omega_{\text{imp}} = E_{\text{imp}} - T S_{\text{imp}}$, of the effective impurity model. The latter can be obtained from $E_{\text{imp}}(T)$, via $C_{\text{imp}}(T)$ and $S_{\text{imp}}(T) = \int_0^T dT' \frac{C_{\text{imp}}(T')}{T'}$. The impurity internal energy, expressed in terms of local dynamical quantities as in Ref. 45, has recently been used in a DMFT solution of the Hubbard model within a variational generalization⁸⁴ of the local moment approach.⁸⁵

In the future, it may be interesting, especially in the context of qubits or nanodevices, to consider the time dependence of the impurity internal energy subject to an initial state preparation, for example, within techniques such as time-dependent density matrix renormalization group^{86–88} or time-dependent NRG.^{33,89,90}

ACKNOWLEDGMENTS

We thank D. P. DiVincenzo, A. Rosch, S. Kirchner, A. Weichselbaum, G.-L. Ingold, P. Hänggi and A. Liebsch for useful discussions and comments on this work, and A. Kauch for drawing our attention to Ref. 45. We acknowledge supercomputer support by the John von Neumann institute for Computing (Jülich).

Appendix A: Band contribution to impurity internal energy

The expression (11) for the conduction band contribution to the impurity internal energy requires evaluation of the integral

$$I(\omega) = \int d\epsilon \frac{\epsilon V^2 N(\epsilon)}{(\omega - \epsilon + i\delta)^2}. \quad (\text{A1})$$

We assume a density of states $N(\omega)$ vanishing at the band edges at $\omega = \pm D$. The hybridization function $\Delta(\omega) =$

$\sum_k V^2/(\omega - \epsilon_k + i\delta) = \Delta_R(\omega) + i\Delta_I(\omega)$ where $\Delta_I(\omega) = -\pi N(\omega)V^2$. With these definitions, we have

$$\begin{aligned} I(\omega) &= -\frac{1}{\pi} \int_{-D}^{+D} d\epsilon \epsilon \Delta_I(\epsilon) \frac{\partial}{\partial \epsilon} \frac{1}{(\omega - \epsilon + i\delta)} \\ &= -\frac{1}{\pi} \frac{\epsilon \Delta_I(\epsilon)}{\omega - \epsilon + i\delta} \Big|_{-D}^{+D} \\ &\quad + \frac{1}{\pi} \int_{-D}^{+D} d\epsilon \frac{1}{\omega - \epsilon + i\delta} \frac{\partial}{\partial \epsilon} (\epsilon \Delta_I(\epsilon)). \quad (\text{A2}) \end{aligned}$$

The first term vanishes since $\Delta_I(\pm D) = 0$ for regular (e.g., 3D) densities of states (and will otherwise result in contributions with negligible temperature dependence). The second term can be evaluated by noting that $\Delta(\omega + i\delta)$ satisfies the causal properties of retarded Green functions and by using the following properties of principle value (P.V.) integrals: if $\text{P.V.}[f(x)] = g(y)$ then $\text{P.V.}[f'(x)] = g'(y)$ and $\text{P.V.}[xf(x)] = yg(y) + \frac{1}{\pi} \int dx f(x)$. The final result is

$$I(\omega) = -\frac{\partial}{\partial \omega} (\omega \Delta(\omega)) \quad (\text{A3})$$

Appendix B: Numerical solution of the Thermodynamic Bethe Ansatz equations

In this Appendix, we summarize the thermodynamic Bethe ansatz (TBA) equations for the Anderson model, which were derived by Okiji and Kawakami^{42,91,92} and Tsvelick, Filyov, and Wiegmann,^{40,41,93,94} and provide details of their numerical solution.^{46–49,62,95} The numerical procedure described applies to both the symmetric and asymmetric Anderson models and in the presence of a finite magnetic field and was used to obtain the results presented in this paper.

1. Thermodynamic Bethe Ansatz Equations

The thermodynamic Bethe ansatz (TBA) produces an infinite set of coupled integral equations for the functions $\epsilon(k)$, $\kappa'_n(\Lambda)$ and $\kappa_n(\Lambda)$, $n = 1, 2, \dots$, describing the charge and spin excitations of the system (Tsvelick and

Wiegmann⁴⁰):

$$\begin{aligned} \epsilon(k) - T \cdot \int_{-\infty}^{\infty} s(g(k) - \Lambda) \cdot \ln(f(\kappa_1(\Lambda))) d\Lambda = \\ \epsilon_0(k) - T \cdot \int_{-\infty}^{\infty} s(g(k) - \Lambda) \cdot \ln(f(\kappa'_1(\Lambda))) d\Lambda \end{aligned} \quad (\text{B1a})$$

$$\begin{aligned} \kappa_n(\Lambda) + T \cdot (s * (\ln(f(\kappa_{n+1})) + \ln(f(\kappa_{n-1}))))(\Lambda) = \\ \delta_{n,1} \cdot T \cdot \int_{-\infty}^{\infty} s(g(k) - \Lambda) \cdot \ln(f(-\epsilon(k))) \cdot g'(k) dk \end{aligned} \quad (\text{B1b})$$

$$\begin{aligned} \kappa'_n(\Lambda) + T \cdot (s * (\ln(f(\kappa'_{n+1})) + \ln(f(\kappa'_{n-1}))))(\Lambda) = \\ \delta_{n,1} \cdot T \cdot \int_{-\infty}^{\infty} s(g(k) - \Lambda) \cdot \ln(f(\epsilon(k))) \cdot g'(k) dk \end{aligned} \quad (\text{B1c})$$

where

$$\begin{aligned} g(k) &= \frac{(k - \varepsilon_d - \frac{1}{2}U)^2}{2\Gamma U}, \quad s(\Lambda) = \frac{1}{2 \cosh(\pi \Lambda)}, \\ f(k) &= \frac{1}{1 + e^{k/T}}, \quad R(x) = \frac{1}{\pi} \int_0^{\infty} \frac{\cos(\omega x)}{1 + e^{\omega}} d\omega \\ \epsilon_0(k) &= k - \varepsilon_d - \frac{1}{2}U + \int_{-\infty}^{\infty} R(g(k) - g(p)) \cdot p \cdot g'(p) dp \end{aligned}$$

$g'(k)$ denotes the first derivative of $g(k)$ with respect to k . $*$ is the convolution of two functions. κ_0 and κ'_0 equal $-\infty$. For $n \rightarrow \infty$ the functions approach the constant values,

$$\lim_{n \rightarrow \infty} \kappa_n = n \cdot H, \quad \lim_{n \rightarrow \infty} \kappa'_n = n \cdot (2\varepsilon_d + U), \quad (\text{B2})$$

where H is a uniform magnetic field and $2\varepsilon_d + U$ measures the deviation from the symmetric point at $\varepsilon_d = -U/2$. The impurity contribution to the specific heat, C_{imp} , may be calculated from the the impurity contribution to the thermodynamic potential, Ω_{imp} , via $C_{\text{imp}} = -T\partial^2\Omega_{\text{imp}}/\partial T^2$, where

$$\begin{aligned} \Omega_{\text{imp}} = T \int_{-\infty}^{\infty} \rho_0(k) \cdot \ln(f(-\epsilon(k))) dk \\ + T \int_{-\infty}^{\infty} \sigma_0(\Lambda) \cdot \ln(\kappa'_1(\Lambda)) d\Lambda + E_0 \end{aligned} \quad (\text{B3})$$

The functions ρ_0 and σ_0 are given by:

$$\begin{aligned} \sigma_0(\Lambda) &= \int_{-\infty}^{\infty} s(\Lambda - g(k)) \cdot \Delta(k) dk \\ \rho_0(k) &= \Delta(k) + g'(k) \cdot \int_{-\infty}^{\infty} R(g(k) - g(p)) \cdot \Delta(p) dp, \end{aligned}$$

where $\Delta(k) = \frac{\Gamma}{\pi(\Gamma^2 + (k - \varepsilon_d)^2)}$. E_0 is the ground state energy of the symmetric Anderson model.⁹¹ Note two changes with respect to the earlier Ref. 40: a sign change in equation B1c (as in Wiegmann and Tsvelick⁴¹) and a

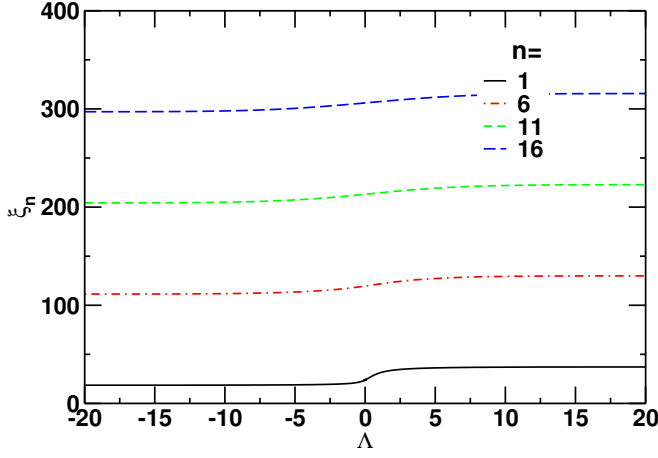


FIG. 14. (Color online) The figure shows a set of ξ_n for the symmetric case ($\varepsilon_d + U/2 = 0$) zoomed to range of $\Lambda = -20 \dots 20$. The functions become smoother with higher n due to the convolution with $s(x)$.

factor 2 in the boundary value for κ'_n in equation B2 (as in Okiji and Kawakami⁴²).

For the calculations we use a transformation of κ_n and κ'_n to new functions ξ_n and ξ'_n similar to that used in previous works.^{46,47,62} After substituting $\xi_n = \ln(1 + e^{\kappa_n/T})$ and $\xi'_n = \ln(1 + e^{\kappa'_n/T})$ we obtain the following coupled equations:

$$\xi_1(\Lambda) = \ln(1 + \exp((s * (\xi_2 + I_1))(\Lambda))) \quad (\text{B4a})$$

$$\xi_n(\Lambda) = \ln(1 + \exp((s * (\xi_{n-1} + \xi_{n+1}))(\Lambda))) \quad (\text{B4b})$$

$$\xi'_1(\Lambda) = \ln(1 + \exp((s * (\xi'_2 + I'_1))(\Lambda))) \quad (\text{B4c})$$

$$\xi'_n(\Lambda) = \ln(1 + \exp((s * (\xi'_{n-1} + \xi'_{n+1}))(\Lambda))) \quad (\text{B4d})$$

$$I_1(\Lambda) = \int_{-\infty}^{\infty} s(g(k) - \Lambda) \cdot \ln(f(-\epsilon(k))) \cdot g'(k) dk \quad (\text{B4e})$$

$$I'_1(\Lambda) = \int_{-\infty}^{\infty} s(g(k) - \Lambda) \cdot \ln(f(\epsilon(k))) \cdot g'(k) dk \quad (\text{B4f})$$

$$I(k) = \int_{-\infty}^{\infty} s(g(k) - \Lambda) \cdot (\xi_1(\Lambda) - \xi'_1(\Lambda)) d\Lambda \quad (\text{B4g})$$

$$e(k) = e_0(k) + T \cdot I(k) \quad (\text{B4h})$$

2. Truncation

For calculational purposes the equations ξ_n and ξ'_n have to be truncated at some finite value $n = N$ and $n' = N'$. One has to calculate the functions at the truncation with care, to avoid wrong results at the boundaries $\Lambda \rightarrow \pm\infty$. We use the truncation scheme of Takahashi and Shiroishi.⁹⁵ It is assumed that the function $s(x)$ can be approximated by $\delta(x)/2$ for large n or n' . This is justified as the functions become smoother in this region (see figure 14). Rewritten for the Anderson Model and

for ξ_N and $\xi'_{N'}$ the corresponding truncation functions are calculated by:

$$\xi_N = \ln \left(\left(\cosh\left(\frac{H}{2}\right) \cdot \sqrt{2 + e^{\xi_{N-1}}} + \sqrt{1 + \sinh^2\left(\frac{H}{2}\right) \cdot [2 + e^{\xi_{N-1}}]^2} \right) \right) \quad (\text{B5a})$$

$$\xi'_{N'} = \ln \left(\left(\cosh\left(\frac{2\varepsilon_d + U}{2}\right) \cdot \sqrt{2 + e^{\xi'_{N'-1}}} + \sqrt{1 + \sinh^2\left(\frac{2\varepsilon_d + U}{2}\right) \cdot [2 + e^{\xi'_{N'-1}}]^2} \right) \right) \quad (\text{B5b})$$

As a further check, and to ensure the correct behaviour at the boundaries, the TBA integral equations were explicitly solved in the limits of $\Lambda, k \rightarrow \pm\infty$. As the functions are smooth in this limit one can assume that $s(x) \rightarrow \delta(x)/2$ and $\lim_{k \rightarrow \infty} \epsilon_0(k) = 2(k - \varepsilon_d - U/2)$, $\lim_{k \rightarrow -\infty} \epsilon_0(k) = 0$. This leads to the following set of coupled algebraic equations:

$$\lim_{\Lambda \rightarrow -\infty} \xi_1 = \ln(1 + \exp(\frac{1}{2}\xi_2)) \quad (\text{B6a})$$

$$\xi_n = \ln(1 + \exp(\frac{1}{2}(\xi_{n-1} + \xi_{n+1}))) \quad (\text{B6b})$$

$$\xi'_1 = \ln(1 + \exp(\frac{1}{2}\xi'_2)) \quad (\text{B6c})$$

$$\xi'_n = \ln(1 + \exp(\frac{1}{2}(\xi'_{n-1} + \xi'_{n+1}))) \quad (\text{B6d})$$

$$\lim_{\Lambda \rightarrow \infty} \xi_1 = \ln(1 + \exp(\frac{1}{2}(\xi_2 - \ln(1 + \exp(\frac{1}{2}\xi_1))))) \quad (\text{B6e})$$

$$\xi_n = \ln(1 + \exp(\frac{1}{2}(\xi_{n-1} + \xi_{n+1}))) \quad (\text{B6f})$$

$$\xi'_1 = 0 \quad (\text{B6g})$$

$$\xi'_n = \ln(1 + \exp(\frac{1}{2}(\xi'_{n-1} + \xi'_{n+1}))) \quad (\text{B6h})$$

The truncation constants ξ_N and $\xi'_{N'}$ are calculated as in equation B5. The boundary values were calculated by iteration using a modification of the Powell hybrid method.

3. Numerical Details

For the calculations, a logarithmic grid was used that is centred around $\varepsilon_d + U/2$. The TBA equations were solved by iteration. The initial values of ξ_n and ξ'_n were chosen to fit a tanh-function with boundary values given by the correct boundary values of ξ_n and ξ'_n , obtained as described above. The integrations were carried out using adaptive routines with the integrands being represented by splines of smooth functions only (see below).

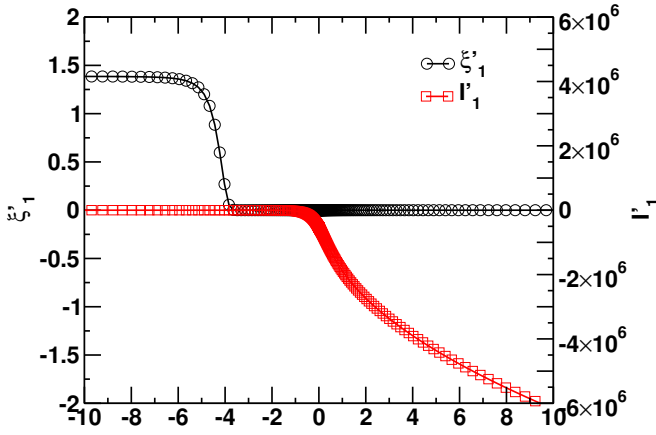


FIG. 15. (Color online) Comparison between I'_1 and ξ'_1 for 500 iterations and $T = 10^{-4}T_K$. Parameters were chosen to be the same as in figure 1. For very low temperatures ξ'_1 (circles, left y -axis) exhibits an exponential drop beyond a certain rapidity Λ_0 (≈ -4 for the case shown) which is difficult to capture with a fixed grid. This problem can be overcome by using the smooth function I'_1 (squares, right y -axis) to calculate ξ'_1 via Eq. (B4c).

A smoother convergence of the iteration procedure is obtained by using 10% of the old iteration values in each step. To represent only smooth functions as splines, ξ_1 and ξ'_1 are not interpolated, but instead the $s * \xi_2$ and $s * \xi'_2$ respectively. The values of ξ_1 and ξ'_1 are then calculated from these convolutions and from I_1 and I'_1 using Eq. (B4a) and Eq. (B4c). This avoids numerical problems due to the exponential drop to zero of ξ'_1 beyond a certain rapidity Λ_0 . See Figure 15 for a comparison between the behavior of ξ'_1 and I'_1 . $N = N' = 20$ functions were used and iterated 500 times for the figures in this section (and 2000 times for the results in the paper). The growth-rate of the grid was 1.05 and it consisted of 801 points. The mid 400 values lie in a range of $[-40, 40]$. After a certain temperature dependent cut-off ($\pm 40 \pm 40 \cdot T/T_0$) the boundary values were used instead of being calculated to ensure numerical stability. The thermodynamic potential was calculated in a range of $T_0 \cdot 10^{-3}$ to $T_0 \cdot 10^6$ on a logarithmic mesh (factor $2^{1/8}$ as step width) where T_0 is defined as $T_0 = \sqrt{UT/2} \cdot \exp(-\frac{\pi U}{8\Gamma} + \frac{\pi \Gamma}{2U})$, Kondo temperature for the symmetric case. It is related to the magnetic susceptibility at zero temperature $\chi_{\text{imp}}(T = 0) = \frac{(g\mu_B)^2}{4k_B T_0}$ (see Hewson in Ref. 1 p. 165, and Kawakami and Okiji in Ref. 96).

- ¹ A. C. Hewson, *The Kondo Problem to Heavy Fermions* (Cambridge University Press, Cambridge, 1997).
- ² A. Zawadowski, *Phys. Rev. Lett.* **45**, 211 (1980).
- ³ A. Caldeira and A. Leggett, *Annals of Physics* **149**, 374 (1983).
- ⁴ A. J. Leggett, S. Chakravarty, A. T. Dorsey, M. P. A. Fisher, A. Garg, and W. Zwerger, *Rev. Mod. Phys.* **59**, 1 (1987).
- ⁵ U. Weiss, *Quantum dissipative systems*, Vol. 13 (World Scientific Pub Co Inc, 2008).
- ⁶ G. Zaránd, *Phys. Rev. B* **72**, 245103 (2005).
- ⁷ D. Loss and D. P. DiVincenzo, *Phys. Rev. A* **57**, 120 (1998).
- ⁸ J. Park, A. Pasupathy, J. Goldsmith, C. Chang, Y. Yaish, J. Petta, M. Rinkoski, J. Sethna, H. Abruña, P. McEuen, and D. Ralph, *Nature* **417**, 722 (2002).
- ⁹ L. H. Yu and D. Natelson, *Nano Letters* **4**, 79 (2004).
- ¹⁰ N. Roch, S. Florens, T. A. Costi, W. Wernsdorfer, and F. Balestro, *Phys. Rev. Lett.* **103**, 197202 (2009).
- ¹¹ J. J. Parks, A. R. Champagne, T. A. Costi, W. W. Shum, A. N. Pasupathy, E. Neuscamman, S. Flores-Torres, P. S. Cornaglia, A. A. Aligia, C. A. Balseiro, G. K.-L. Chan, H. D. Abruña, and D. C. Ralph, *Science* **328**, 1370 (2010).
- ¹² D. Goldhaber-Gordon, J. Göres, M. A. Kastner, H. Shtrikman, D. Mahalu, and U. Meirav, *Phys. Rev. Lett.* **81**, 5225 (1998).
- ¹³ S. M. Cronenwett, T. H. Oosterkamp, and L. P. Kouwenhoven, *Science* **281**, 540 (1998).
- ¹⁴ A. V. Kretinin, H. Shtrikman, D. Goldhaber-Gordon, M. Hanl, A. Weichselbaum, J. von Delft, T. Costi, and D. Mahalu, *Phys. Rev. B* **84**, 245316 (2011).
- ¹⁵ J. Nygard, D. Cobden, and P. Lindelof, *Nature* **408**, 342 (2000).
- ¹⁶ V. Madhavan, W. Chen, T. Jamneala, M. Crommie, and N. Wingreen, *Science* **280**, 567 (1998).
- ¹⁷ A. Otte, M. Ternes, K. Von Bergmann, S. Loth, H. Brune, C. Lutz, C. Hirjibehedin, and A. Heinrich, *Nature Physics* **4**, 847 (2008).
- ¹⁸ J. Li, W.-D. Schneider, R. Berndt, and B. Delley, *Phys. Rev. Lett.* **80**, 2893 (1998).
- ¹⁹ W. Metzner and D. Vollhardt, *Phys. Rev. Lett.* **62**, 324 (1989).
- ²⁰ A. Georges, G. Kotliar, W. Krauth, and M. J. Rozenberg, *Rev. Mod. Phys.* **68**, 13 (1996).
- ²¹ G. Kotliar and D. Vollhardt, *Physics Today* **57**, 53 (2004).
- ²² D. Vollhardt, *Annalen der Physik* **524**, 1 (2012).
- ²³ K. G. Wilson, *Rev. Mod. Phys.* **47**, 773 (1975).
- ²⁴ H. R. Krishna-murthy, J. W. Wilkins, and K. G. Wilson, *Phys. Rev. B* **21**, 1003 (1980).
- ²⁵ H. R. Krishna-murthy, J. W. Wilkins, and K. G. Wilson, *Phys. Rev. B* **21**, 1044 (1980).
- ²⁶ R. Bulla, T. A. Costi, and T. Pruschke, *Rev. Mod. Phys.* **80**, 395 (2008).
- ²⁷ L. N. Oliveira and J. W. Wilkins, *Phys. Rev. Lett.* **47**, 1553 (1981).
- ²⁸ H. O. Frota and L. N. Oliveira, *Phys. Rev. B* **33**, 7871 (1986).
- ²⁹ O. Sakai, Y. Shimizu, and T. Kasuya, *Journal of the Physical Society of Japan* **58**, 3666 (1989).
- ³⁰ T. A. Costi and A. C. Hewson, *Philosophical Magazine Part B* **65**, 1165 (1992).
- ³¹ R. Bulla, A. C. Hewson, and T. Pruschke, *Journal of Physics: Condensed Matter* **10**, 8365 (1998).
- ³² W. Hofstetter, *Phys. Rev. Lett.* **85**, 1508 (2000).
- ³³ F. B. Anders and A. Schiller, *Phys. Rev. Lett.* **95**, 196801 (2005).

- ³⁴ R. Peters, T. Pruschke, and F. B. Anders, *Phys. Rev. B* **74**, 245114 (2006).
- ³⁵ A. Weichselbaum and J. von Delft, *Phys. Rev. Lett.* **99**, 076402 (2007).
- ³⁶ T. A. Costi, A. C. Hewson, and V. Zlatić, *J. Phys.: Condens. Matter* **6**, 2519 (1994).
- ³⁷ C. Gonzalez-Buxton and K. Ingersent, *Phys. Rev. B* **57**, 14254 (1998).
- ³⁸ H. v. Löhneysen, A. Rosch, M. Vojta, and P. Wölfle, *Rev. Mod. Phys.* **79**, 1015 (2007).
- ³⁹ S. C. Costa, C. A. Paula, V. L. Líbero, and L. N. Oliveira, *Phys. Rev. B* **55**, 30 (1997).
- ⁴⁰ A. M. Tsvelick and P. B. Wiegmann, *Physics Letters A* **89**, 368 (1982).
- ⁴¹ P. B. Wiegmann and A. M. Tsvelick, *Journal of Physics C: Solid State Physics* **16**, 2281 (1983).
- ⁴² A. Okiji and N. Kawakami, *Phys. Rev. Lett.* **50**, 1157 (1983).
- ⁴³ Y. Nagaoka, *Phys. Rev.* **138**, A1112 (1965).
- ⁴⁴ P. E. Bloomfield and D. R. Hamann, *Phys. Rev.* **164**, 856 (1967).
- ⁴⁵ B. Kjollerström, D. J. Scalapino, and J. R. Schrieffer, *Phys. Rev.* **148**, 665 (1966).
- ⁴⁶ V. T. Rajan, J. H. Lowenstein, and N. Andrei, *Phys. Rev. Lett.* **49**, 497 (1982).
- ⁴⁷ H.-U. Desgranges, *Journal of Physics C: Solid State Physics* **18**, 5481 (1985).
- ⁴⁸ P. D. Sacramento and P. Schlottmann, *Phys. Rev. B* **43**, 13294 (1991).
- ⁴⁹ C. J. Bolech and N. Andrei, *Phys. Rev. B* **71**, 205104 (2005).
- ⁵⁰ W. C. Oliveira and L. N. Oliveira, *Phys. Rev. B* **49**, 11986 (1994).
- ⁵¹ V. L. Campo and L. N. Oliveira, *Phys. Rev. B* **72**, 104432 (2005).
- ⁵² J. B. Silva, W. L. C. Lima, W. C. Oliveira, J. L. N. Mello, L. N. Oliveira, and J. W. Wilkins, *Phys. Rev. Lett.* **76**, 275 (1996).
- ⁵³ V. L. Campo and L. N. Oliveira, *Phys. Rev. B* **70**, 153401 (2004).
- ⁵⁴ J. V. B. Ferreira, A. I. I. Ferreira, A. H. Leite, and V. L. Líbero, *Journal of Magnetism and Magnetic Materials* **324**, 1011 (2012).
- ⁵⁵ P. W. Anderson, *Physical Review* **124**, 41 (1961).
- ⁵⁶ J. R. Schrieffer and P. A. Wolff, *Phys. Rev.* **149**, 491 (1966).
- ⁵⁷ G. Iche and A. Zawadowski, *Solid State Communications* **10**, 1001 (1972).
- ⁵⁸ A. C. Hewson, J. Bauer, and W. Koller, *Phys. Rev. B* **73**, 045117 (2006).
- ⁵⁹ L. R. Ramos, W. C. Oliveira, and V. L. Líbero, *Phys. Rev. B* **67**, 085104 (2003).
- ⁶⁰ F. Guinea, V. Hakim, and A. Muramatsu, *Phys. Rev. B* **32**, 4410 (1985).
- ⁶¹ T. A. Costi and C. Kieffer, *Phys. Rev. Lett.* **76**, 1683 (1996).
- ⁶² T. A. Costi and G. Zarand, *Physical Review B* **59**, 12398 (1999).
- ⁶³ T. A. Costi, *Phys. Rev. Lett.* **80**, 1038 (1998).
- ⁶⁴ R. Görlich and U. Weiss, *Phys. Rev. B* **38**, 5245 (1988).
- ⁶⁵ N. Chandra, M. Kollar, and D. Vollhardt, *Phys. Rev. B* **59**, 10541 (1999).
- ⁶⁶ T. A. Costi and R. H. McKenzie, *Phys. Rev. A* **68**, 034301 (2003).
- ⁶⁷ K. L. Hur, *Annals of Physics* **323**, 2208 (2008).
- ⁶⁸ S. Florens, A. Freyn, D. Venturelli, and R. Narayanan, *Phys. Rev. B* **84**, 155110 (2011).
- ⁶⁹ P. Hänggi and G.-L. Ingold, *Acta Physica Polonica B* **37**, 1537 (2006).
- ⁷⁰ P. Hänggi, G.-L. Ingold, and P. Talkner, *New Journal of Physics* **10**, 115008 (2008).
- ⁷¹ G.-L. Ingold, P. Hänggi, and P. Talkner, *Phys. Rev. E* **79**, 061105 (2009).
- ⁷² G. Ingold, *The European Physical Journal B-Condensed Matter and Complex Systems* **85**, 1 (2012).
- ⁷³ G. W. Ford and R. F. O'Connell, *Physica E: Low-dimensional Systems and Nanostructures* **29**, 82 (2005).
- ⁷⁴ H. Hasegawa, *Journal of Mathematical Physics* **52**, 123301 (2011).
- ⁷⁵ H. B. Callen, *Thermodynamics and an Introduction to Thermostatistics* (John Wiley & Sons, New York, 1985).
- ⁷⁶ S. Florens and A. Rosch, *Phys. Rev. Lett.* **92**, 216601 (2004).
- ⁷⁷ R. Žitko and T. Pruschke, *Phys. Rev. B* **79**, 012507 (2009).
- ⁷⁸ M. Vojta and R. Bulla, *The European Physical Journal B-Condensed Matter and Complex Systems* **28**, 283 (2002).
- ⁷⁹ E. Gull, A. J. Millis, A. I. Lichtenstein, A. N. Rubtsov, M. Troyer, and P. Werner, *Rev. Mod. Phys.* **83**, 349 (2011).
- ⁸⁰ J. E. Hirsch and R. M. Fye, *Phys. Rev. Lett.* **56**, 2521 (1986).
- ⁸¹ A. Liebsch and H. Ishida, *Journal of Physics: Condensed Matter* **24**, 053201 (2012).
- ⁸² E. Jakobi, N. Blümer, and P. van Dongen, *Phys. Rev. B* **80**, 115109 (2009).
- ⁸³ V. Janiš, *Zeitschrift für Physik B Condensed Matter* **83**, 227 (1991).
- ⁸⁴ A. Kauch and K. Byczuk, *Physica B: Condensed Matter* **407**, 209 (2012).
- ⁸⁵ D. E. Logan, M. P. Eastwood, and M. A. Tusch, *Journal of Physics: Condensed Matter* **10**, 2673 (1998).
- ⁸⁶ A. J. Daley, C. Kollath, U. Schollwöck, and G. Vidal, *Journal of Statistical Mechanics: Theory and Experiment* **2004**, P04005 (2004).
- ⁸⁷ S. R. White and A. E. Feiguin, *Phys. Rev. Lett.* **93**, 076401 (2004).
- ⁸⁸ L. G. G. V. Dias da Silva, F. Heidrich-Meisner, A. E. Feiguin, C. A. Büsser, G. B. Martins, E. V. Anda, and E. Dagotto, *Phys. Rev. B* **78**, 195317 (2008).
- ⁸⁹ T. A. Costi, *Phys. Rev. B* **55**, 3003 (1997).
- ⁹⁰ A. Rosch, *The European Physical Journal B-Condensed Matter and Complex Systems* **85**, 1 (2012).
- ⁹¹ N. Kawakami and A. Okiji, *Physics Letters A* **86**, 483 (1981).
- ⁹² N. Kawakami and A. Okiji, *Journal of the Physical Society of Japan* **51**, 2043 (1982).
- ⁹³ A. M. Tsvelick and P. B. Wiegmann, *Journal of Physics C: Solid State Physics* **16**, 2321 (1983).
- ⁹⁴ V. M. Filyov, A. M. Tsvelick, and P. B. Wiegmann, *Physics Letters A* **89**, 157 (1982).
- ⁹⁵ M. Takahashi and M. Shiroishi, *Phys. Rev. B* **65**, 165104 (2002).
- ⁹⁶ N. Kawakami and A. Okiji, *Solid State Communications* **43**, 467 (1982).